MICROSTRUCTURE DEVELOPMENT AND EVOLUTION OF SPUTTER DEPOSITED INDIUM THIN FILMS IN CRYOGENICS

Except where reference is made to the work of others, the work described in this thesis is my own or was done in collaboration with my advisory committee. This thesis does not include proprietary or classified information.

Jung Hyun Park

Certificate of Approval:

Barton C. Prorok
Assistant Professor
Materials Engineering

Dong Joo Kim, Chair
Assistant Professor
Materials Engineering

ZhongYang Cheng
Assistant Professor
Materials Engineering

George T. Flowers
Interim Dean
Graduate School

MICROSTRUCTURE DEVELOPMENT AND EVOLUTION OF SPUTTER DEPOSITED INDIUM THIN FILMS IN CRYOGENICS

Jung Hyun Park

A Thesis

Submitted to

the Graduate Faculty of

Auburn University

in Partial Fulfillment of the

Requirement for the

Degree of

Master of Science

Auburn, Alabama
Aug 04, 2007

MICROSTRUCTURE DEPENDENT AND EVALUATION OF SPUTTERED INDIUM

THIN FILMS IN CRYOGENICS

Jung Hyun Park

Signature of Author

Date of Graduation

VITA

Jung-Hyun Park, son of Kyu-Jick Park and Young-Joo Yoo, was born on September 8, 1974. He attended In-Ha University, Incheon, Korea and obtained a B.S. degree in Metallurgical Engineering in 1997. After working on Ordnance department in Republic of Korea military and Samsung motor company, he entered Auburn University and joined Dr. Kim’s lab in fall 2004.

THESIS ABSTRACT

MICROSTRUCTURE DEVELOPMENT AND EVOLUTION OF SPUTTER DEPOSITED INDIUM THIN FILMS IN CRYOGENICS

Jung Hyun Park

Master of Science, Aug 04, 2007
(B.S. Metallurgical Engineering, In-ha University, South Korea, 1997)

88 Typed Pages

Directed by Dong-Joo Kim

Low melting temperature materials have been deposited on amorphous substrate using DC magnetron sputter system. Process parameters such as power, pressure, and temperature have been investigated to improve surface morphology based on kinetic concept of condensation film mechanisms. Very rough surface was produced in thin films whose thickness was less than 1 micrometer deposited at room temperature, and it seems to correlate with intrinsic stress induced by sputter deposition. Since intrinsic stress is influenced by the diffusion of atoms, microstructure of films could be modified by changing process parameters. Low diffusivity and high nucleation rate created smoother surface with small grain size. Temperature is the most critical parameter that affects nucleation and diffusion of adatoms, so that microstructure could be dramatically modulated at low homologous (Ts/Tm) temperature with nano-granular structure. Indium films were deposited on cooled substrate by flowing liquid nitrogen to obtain low homologous temperature of indium which has low melting temperature as 156 ^{o}C. A structure zone model was proposed with revision for a very thin film of low melting temperature materials, and the boundary between zone 1 and zone 2 was shifted to higher homologous temperature.

Properties due to modulated microstructure were also studied. Sheet resistance and reflectance were dramatically improved in 200 nm thickness films by improved surface roughness. This study provides a better understanding of very thin film deposition, and the wide selection of materials for various applications such as metallic narrow band pass filters, electrodes in flexible display, and so on.

ACKNOWLEDGMENTS

I would like to express my respect and thanks to my advisor Dr. Dong-Joo Kim for his direction, patience, and encouragement which was invaluable during the entire time of this research. I am very grateful for the achive support of Dr. Barton C. Prorok and Dr. ZhongYang Cheng being on my thesis committee. I appreciate my research group members, Sang H. Yoon, Dongna Shen, Dan Liu, Chiwon Kang, and Dr. Joo-Won Lee, for their support and friendship. Finally, I give my sincere appreciation to my wife and daughter for their love and understanding, and to my father and mother for providing help in numerous ways.

Style manual or journal used Guide to Preparation and Submission of Theses and Dissertations

Computer software used Microsoft Word 2003, Origin 7.5, Endnote 8

TABLE OF CONTENTS

LIST OF TABLES

LIST OF FIGURES

CHAPTER 1

INTRODUCTION

1.1 Overview

Very thin films have been widely used in various applications such as optics, electronics, and mechanics with advanced film properties. Integrated circuit (IC) requires thin films that have smooth surface and high density without defects such as impurities, voids, and grain boundaries to prevent the electromigration effect [1]. The narrow band pass filter uses metallic films that have pass band in range extreme ultraviolet regions. Optical filters also demand thin films with smooth, defect-free, and bulk-like microstructure [2-4]. Soft metallic material which has a low melting temperature is one of the materials for such applications. Indium was chosen for this study and prepared by sputter deposition. Indium thin films below 1 μm thickness show very rough surface morphology, which will cause reliability issues in many applications. Therefore, its microstructure was modulated and characterized by changing process parameters considering kinetics of nucleation and growth mechanism of thin film growth. Nucleation and growth in film formation result in a microstructure that includes grain size, density of film, and surface morphology. Deposition rate and diffusion of atoms by the surface or bulk of deposited film mostly control the balance between nucleation and growth in film formation. As the deposition rate is faster with more impinging atoms on the surface, grain size is reduced by the nucleation dominant process with its high rate. The deposition rate can be increased from applied high power on the cathode with increasing bias between cathode and substrate. A smaller distance between them can also increase the deposition rate within geometrical effect of glow discharge. Collisions between target atoms and working gas reduce the kinetic energy of adatoms, so that chamber pressure during deposition affects the surface diffusion of adatoms. Moreover, collisions induce a shadowing effect by impingement of atoms at normal angle cathode to substrate in random direction.

Varing temperature during sputtering can modulate microstructure effectively by diffusion control in film formation. Since indium film deposited at room temperature has high homologous temperature (Ts/Tm) due to its low melting temperature, it has a limit to control its structure by valuable parameter of substrate temperature. The cooling stage was self-manufactured, and it allowed an investigation of a broad range of growth characteristics of this system. Using cryogenic temperature cooled by liquid nitrogen on the indium system leads to homologous temperature (Ts/Tm= 0.4) at -110 ^{o}C. Nano-granular structure was obtained, and columnar grains growth did not occur in this deposition. It is supposed that impurity led to renucleation during thickening stage, but no well-distributed impurity in film has been detected by energy dispersive spectrometer (EDS) analysis. It is not well understood that fine granular structure is produced with restricting columnar grain growth at a vertical direction to surface. Besides the effects of nucleation and growth rate on the surface roughness of films, rough indium films prepared at higher homologous temperatures contain an array of hillocks, and high aspect ratio hillocks that seem to result from lattice diffusion by compressive stress on film [5].

Compressive stress is believed to have derived from thermal expansion stress and intrinsic stress during deposition. Compressive strain was defined in indium films by XRD characterization.

Sheet resistance and reflectance were measured for each film, and their values are saturated after percolation thickness. When comparing films deposited at room temperature and cryogenics, lower resistance and much higher reflectance were indicated at later films even in film thinner (200~400 nm) than 1 µm thick film deposited at room temperature. Although a larger portion of grain boundary areas in the films grown at cryogenic temperature can degrade both values, their smooth surface is believed to improve resistance and reflectance as compared to films deposited at room temperature.

Although there exists an inconsistency between microstructure of theoretical models and process parameters due to their diversity such as deposition method, material system, and others, SZMs can inform us of the initial step and direction to obtain the desired physical microstructure by thin film deposition. In this study, SZM for low melting temperature materials was proposed, and shifted boundary and surface morphology was found from Grovenor's SZM [6]. This revised SZM may account for the structural change in thinner films with low melting points, such as In, Sn, and so on.

1.2 Thesis structure

Chapter 2 includes a literature survey from which this thesis work is based. Applications are introduced in detail, and sputter deposition systems are studied in their physical mechanism and operational parameters. Basic film growth mechanisms that include nucleation, coarsening, coalescence, and thickening are briefly explained with factors that affect microstructure of polycrystalline structure. Theoretical concepts of kinetic and thermodynamic are reviewed with nucleation rate and growth mode. Representative SZMs are explained, and film stress has been deeply studied. Stress analysis can be performed by an XRD test using strain induced by stress.

Chapter 3 shows sample preparation, specifications of the sputtering system, and the characterization of film by XRD, SEM, AFM, reflectance measurement, and four-point probe.

Chapter 4 and chapter 5 discuss results and their analysis, and summarize the above mentioned chapters.

CHAPTER 2

GENERAL BACKGROUND

2.1 Microstructure’s role in thin film properties

Electrical, optical, mechanical, and magnetic properties and the performance of thin films are largely understood through their microstructure such as grain size, grain shape, packing density, lattice defects and void, surface roughness, and crystallographic orientation. These predominant factors appear in thin films due to their volume dependent properties and dependency upon the surface conditions of neighboring solid substrate.

Most metallic films are crystallized with a grain structure called polycrystalline through a various films deposition method in order to organize numerous atoms releasing energy from itself [7, 8]. The method of releasing energy and their magnitude in thin film were estimated by Harper and Rodbell, and are shown in Figure 1.

Polycrystalline metallic films have various applications in the field that includes interconnect material in integrated circuits (IC), optical filters, elements in magnetic devices, catalyst, coatings of wear resistance, and decorative coatings. For complete work on thin film engineering, it must first be interpreted how the microstructure acts on its applied field electrically, optically, or physically.

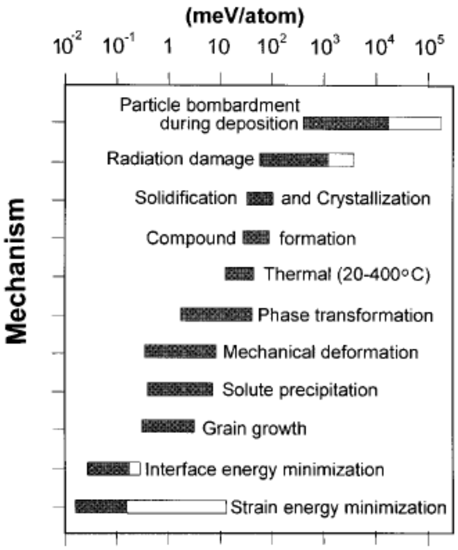

Figure 2.1: Sources of energy available to control thin film microstructure [7]

2.1.1 Metallization

Copper, Aluminum, and their alloys are used for the interconnections of integrated circuits due to their low resistivity of 1.68 ~ 2.65 μΩ-cm. Thin film of interconnections can stand under much higher current density than that of bulk because of heat dissipation through its substrate. In spite of its well-behaved electrical properties, electromigration transfers metal ion cores by electron momentum, and results in mechanical damage such as void formation, mass pileups, hillocks, and failure. This phenomenon is dominately related to the grain boundary (GB) that activates GB channel diffusion of mass. Mass is moving along the GB where involves many voids, and moving in and out of the mass to junction of GB induce difference in their amount. If entrance to this region is much higher than that of exit, mass is piled up near the GB to create hillock. A void is generated in vice versa. Phenomenon of electromigration is illustrated in Figure 2.2. These mechanical deformations cause localized heat and opening the circuit by bridging two conductors [9]. Now Al-Cu alloy is used as interconnection to improve the resistance to electromigration failure. It seems that a small percent of copper enhances the (111) orientation in solvent Al. Although it is not yet well explained that the addition of a small fraction of copper leads to resisting electromigration failure, it is obvious that the changed microstructure results in this improvement. Moreover, the microstructure can be modulated by deposition technique parameters.

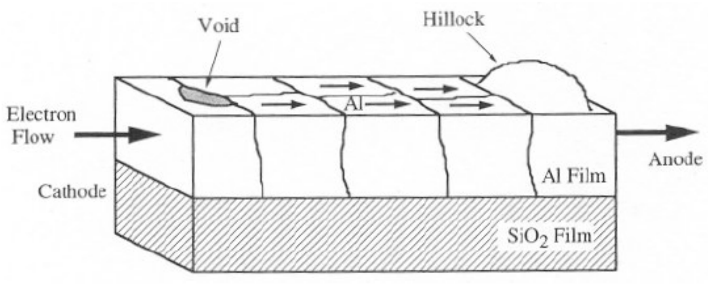

Figure 2.2: Schematic illustration of electromigration. Void and hillock are generated near the grain boundaries [8, 10]

2.1.2 Optical filters

It is well known that thin film technology has been developed to modify the optical properties of thousand of applications such as solar cell, integrated optic, beam splitter, medical electronic, and solar blind filter. One of the promised applications is antireflection (AR) coatings that maximize transmission of the desired wavelength range, and reduce the reflection of others. Multilayer AR coating can be designed to obtain widely transmitted wavelength range, and enhance the reflection. Narrow band pass filter (NBPF) for extreme ultra violet (EUV) interval might be designed with a single or a few layers of thin metallic film. Al, Mg, In, Sn, Mo, and their multilayers are applicable materials in narrow band pass filters in EUV region, and some of them are already commercialized. A distinguished narrow pass band of single or multilayer of metallic films are shown in figure 2.3.

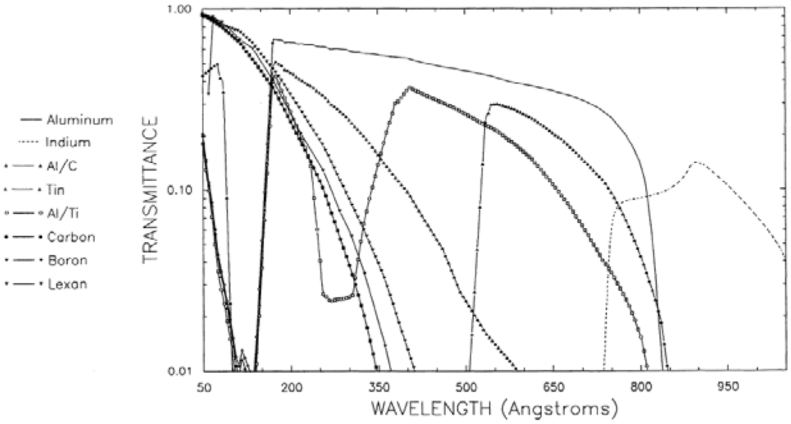

Figure 2.3: Transmittance of different metallic films [11]

A single and multi-layers of antireflection filters can be designed with estimated reflection and transmission that are determined by material selection and layer structure. The optical filter design is based on the innate properties of bulk material, and is calculated by Drude (Equation 2.1) and Lorentz (Equation 2.2) Equations.

$$n^2-k^2=\varepsilon_1=1-\frac{\nu_1^2}{\nu^2+\nu_2^2} \quad \text{and} \quad 2nk=\varepsilon_2=\frac{\nu_2}{\nu}\frac{\nu_1^2}{\nu^2+\nu_2^2}$$

$$\varepsilon_1=n^2-k^2=1+\frac{e^2mN_a}{\varepsilon_o}\sum_i\frac{f_i(\nu_{0i}^2-\nu^2)}{4\pi^2m^2(\nu_{0i}^2-\nu^2)^2+\gamma_i'^2\nu^2} \qquad (2.1)$$

and

$$\varepsilon_2=2nk=\frac{e^2N_a}{2\pi\varepsilon_o}\sum_i\frac{f_i\nu\gamma_i'}{4\pi^2m^2(\nu_{0i}^2-\nu^2)^2+\gamma_i'^2\nu^2} \qquad (2.2)$$

where $v_1 = \sqrt{\frac{e^2 N_f}{4\pi^2 \varepsilon_o m}}$, $v_2 = \frac{2\pi\varepsilon_o v_1^2}{\sigma_o}$, ε_1 is absorption, ε_2 is polarization, n is index of refraction, k is damping constant, v_1 is plasma frequency, v_2 is damping frequency, γ is damping factor, e is electron charge, m is electron mass, N_f is free electrons per cubic centimeter, ε_o is permittivity of empty space, σ_o is d.c. conductivity, N_a is number of atoms per unit volume, and f_a is oscillator strength of i oscillators [12].

Thin film is formed by preferred deposition techniques regarding as estimated optical film design. As thin film has divergence between practice and theory based on bulk materials due to its built-up microstructure, further study of microstructure on optical thin films has been performed. Modeling of optical film design assumes that thin film has a homogeneous and uniform microstructure with well-estimated optical constants such as reflective index (n) and extinction coefficient (k). Real thin film has, however, various sources of inhomogeneous reflective index due to scattering on structural defects [13]. Most thin films show columnar structure that involves porous defects and rough interfaces where incident light scatters and deviates from theoretical values of the optical constant. This scattering is illustrated in Figure 2.4.

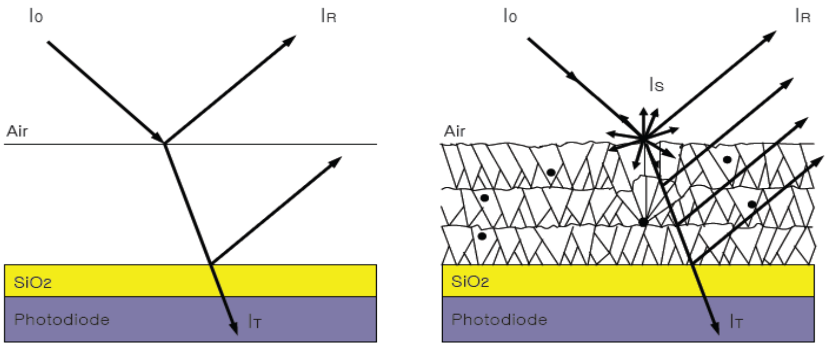

Figure 2.4: Comparison of light scattering due to microstructure defects between theoretic and practical optical thin film

Inhomogeneity can be defined by packing density that has a value of unity in an ideal single layer of thin film. Although it is not well understood that optical properties are influenced by the microstructure of thin film both qualitatively and quantitatively, optical properties of reflective index, reflectivity, light scattering, and surface plasmon are more or less affected by structural defects, called inhomogeneity [14]. The ratio of solid volume to total volume includes voids, called packing density p, suggested to be a major source of deviation from the ideal reflective index suggested by Guenther. Modulating reflective index with regard to packing density has been studied to rectify the practice value in calculation, and the resulted reflectivity was shown to be in agreement with theoretical results [15]. Also, incident light to thin films can be scattered due to its rough surface [16], microscopic shrapnel or rocks [17], and macroscopic nodules and pinholes [18].

In optical applications of thin film, designing the filter structure and manipulating optical properties with regard to aberration caused from microstructure is a significant process. But modulating and improving the microstructure in fabricating steps should be carefully considered to reduce deviation from calculated optical properties. For example, a smooth surface and less grain boundary structure can be controlled by optimized deposition parameters, and high energetic adatoms in physical vapor deposition (PVD) gives more kinetic diffusion at the substrate surface to decrease voids in 3-D film structure. Moreover, ion-assisted deposition technique dramatically improves voidless film properties in approximation to the ideal one.

2.2 Thin film deposition

Various thin film deposition techniques are applied in current technologies using physical and chemical processes. Three useful techniques in thin film formation are presented as evaporation, sputtering deposition, and chemical vapor deposition (CVD). In this section, there is an overview of sputtering fundamentals, and of the perception of the relationship between process parameters and film stress. Sputtering systems usually use plasma which is a basic mechanism of thin film deposition. The plasma can be produced by introducing the gas into high temperatures induced by laser heating, electron beam heating, or shock waves. Also strong electric and magnetic fields can generate plasma, which is the so-called cold plasma that is used in the sputtering process.

2.2.1 Fundamentals of Sputtering

Sputtering is one of the physical vapor deposition (PVD) based on vacuum conditions where positively ionized gas molecules in glow discharge strike a target and their momentum ejects target atoms and transfers them to substrate materials. Typically, argon is used as an inert gas due to its inactivity and heavy atomic weight. After the chamber is pumped down to a pressure in a range between 10^{-4} and 10^{-7}, chamber is backfilled more than 1 mTorr ~ 100 mTorr with inert gas[7]. It is partially ionized by ignition of electric discharge, and that is the so-called glow discharge or plasma.

Target and grounded substrate are biased by applying several kilovolts at target to generate plasma, and the substrate is relatively biased as positive to target bias. They are called cathode and anode respectively. Positively ionized inert gas in plasma induces an ion current, and causes sputtering of target materials and condensation of target atoms on the substrate.

Magnetron enhanced cathode produces a higher deposition rate with a higher current of ions in few order of magnitude. Modulated electric and magnetic fields restrict secondary electrons during bombardment of ionized inert gas to target, and increase the probability of ionizing working gas. They enable, hence, generating and maintaining plasma in lower gas pressure and operation voltage than non-magnetron sputtering. Also, sputtering at low chamber pressure reduces collision until adatoms impinges substrate, with directional randomness of flux. Permanent magnets are installed at the backside in parallel to the target in Figure 2.5.

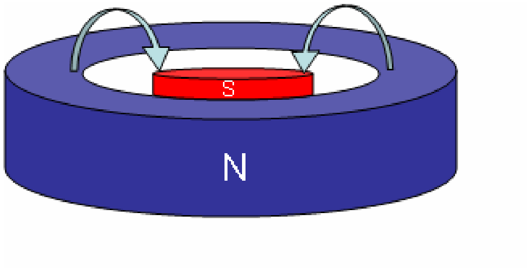

Figure 2.5: Magnetron cathode

Table 2.1: Comparing sputtering system with evaporation deposition system

Evaporation	Sputtering
Low energy atoms (few eV)	Higher energy atoms (5~20 eV)
High vacuum path	Low vacuum, plasma path
- few collisions	- Many collisions

- Line of sight deposition	- Less line of sight deposition
- Little gas in film	- Gas in film
Few parameter selection	Various parameter selection
Limited target selection	Versatile target selection
Poorer adhesion	Better adhesion

Table 2.1 shows characteristics of a sputtering system compared with an evaporation system. Since sputtering has high energy atoms is peening effect on surface of substrate, adhesion is better than in an evaporation system. By selection of versatile processing parameters, microstructure modulation can be obtained in wide range.

Any material can be chosen in a sputtering system due to its selection of type of power such as DC, RF, and advanced compound film can be obtained by reactive sputtering by supplying reactive gas during deposition.

2.2.2 Plasma fundamentals

Plasma is energetically the fourth state of matter after the solid, liquid, and gas phases. While thermal plasma generates high temperature gas with thermodynamic equilibrium, cold plasma in low pressure maintains the gas at room temperature. Cold plasma used in a sputtering system is a conducting medium within a low-pressure gas phase and voltage distribution between two electrodes, shown in Figure 2.6 [7]

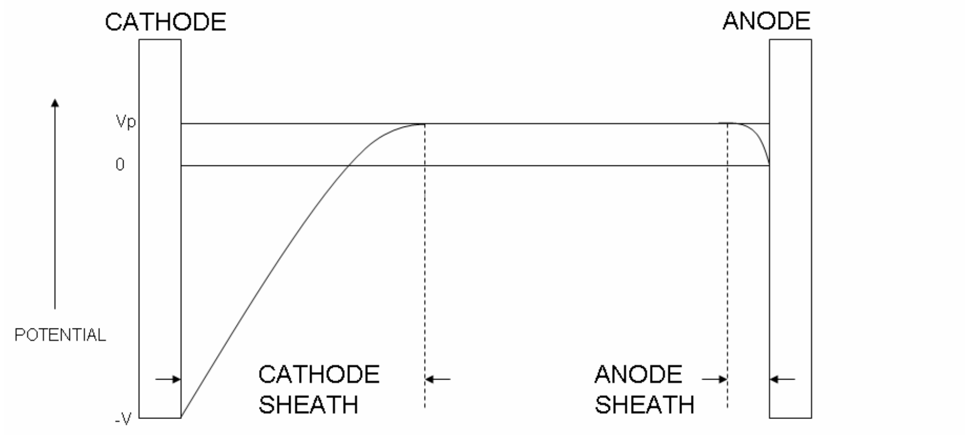

Figure 2.6: Voltage distribution across DC glow discharge [7]

When voltage starts to be applied, very small currents flow by small number of free charges that are generated by the background cosmic radiation and collected. As the voltage increases, created charged particles by ionization of inert gas steadily increase the current and voltage is saturated at a certain point set up by output impedance of the power supply. This region is named the Townsend Discharge where voltage is constant and current increases. The voltage at the Townsend Discharge stage is beakdown voltage to create glow discharge. The reasons for this avalanche process are toe create secondary electrons from cathode and neutral atoms of inert gas, and fresh ions repeat the process.

As the number of electrons increase and the rate of recombination reaches to equilibrium with formation of ions, glow discharge starts to be generated with voltage drop and the abrupt increasing of the current. This stage is the so-called normal glow. At this stage, the discharge partially covers the edge of the cathode, since there is not enough power for ion bombardment of the cathode to cover the entire cathode. When the glow covers the entire cathode with raised power, voltage is increased with current with starting sputtering processes. This stage is called abnormal discharge. Further increase of power leads to the formation of arcs and heating cathode. Above mechanisms are illustrated in a diagram in see Figure 2.7.

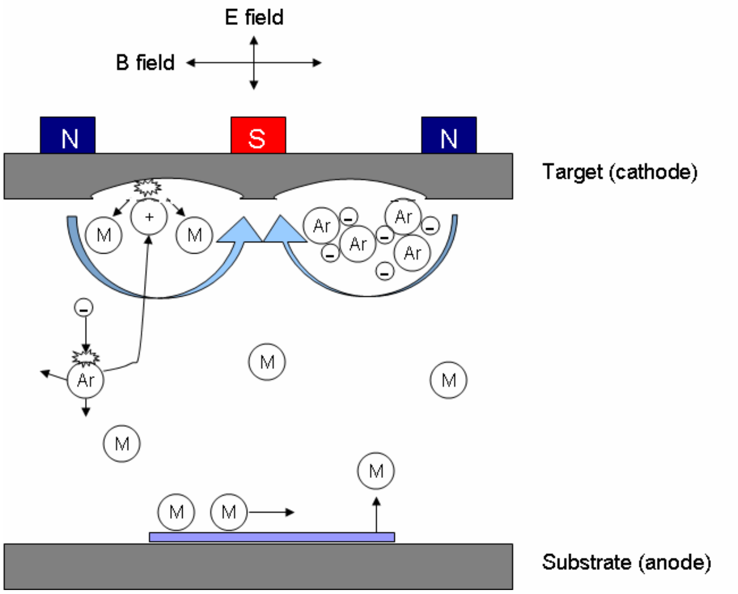

Figure 2.7: schematic diagram of magnetron sputtering mechanism

Plasma is talent material in thin film deposition, and the microstructure can be modulated by changing parameters of power, pressure, bias, and substrate temperature. More information of plasma can be obtained in reference [19].

2.3 Film growth mechanism summary

Most metallic films form a polycrystalline microstructure, and they demonstrate us most of their properties in various applications such as in electronic, magnetic, photonic, and micromechanical. Although many complex and specific variables in deposition configuration and materials class affect film formation, it is well known that the general trend of film formation is established with fundamentals of kinetics and thermodynamics.

In other words, film formation is an energy relief process during deposition with some mechanisms such as grain boundary formation, grain growth, deformation, phase transformation, and so on as shown in Figure 2.1. Nucleation, coarsening, coalescence, and thickening can be interpreted by the energy of atoms at the condensation of solid film from a vapor phase. Kinetic and thermodynamic concepts are complementary to each other to understand film formation mechanisms, and structure zone models (SZMs) attest and supplement by experimental data.

Table 2.2: Factors affecting microstructure of polycrystalline structure [20]

- Kinetic factors affecting structure evolution
  - Adatom diffusivities on the substrate surface
  - Adatom self-diffusivities on island surfaces
  - Self-diffusivities in grain boundaries
  - Grain boundary mobilities
  - Adatom cluster nucleation rates
  - Adatom desorption rates
- Process parameters
  - Deposition rate (affects adatom arrival rate, affects adatom diffusion time before cluster nucleation or desorption, affects film purity)
  - Substrate temperature (affects all kinetic processes, increasing rates with increasing temperature
  - Background pressure (affects film and surface purity)
  - In sputter deposition: sputtering gas pressure and substrate bias (affect the angular distribution and energies of arriving adatoms)
- Factors affecting zone models
  - Materials class
  - Impurities incorporation
  - Deposition technique

Table 2.2 summarizes factors affecting the microstructure evolution of thin film in kinetic concept and process parameters [20]. As shown in kinetic factors, all factors are related to diffusivity of adatoms with their bonding energy on the surface of the neighboring surface, if duration time of deposition is long enough. Neglecting background pressure concerned with impurity, deposition rate is not a term of the diffusivity of atoms, but can restrict diffusion of atoms with time limitation.

2.3.1 Film formation

Normal film formation is constructed by nucleation, grain growth, and thickening after reach to continuous film. After nucleation was established, formed nuclei grow by expansion into external phase with forming bigger islands or coarsening during coalescence which is the impingement of islands. Grain growth is dependent on substrate temperature as well as deposition rate, and grain size will be larger by increasing both of them. Their quantitative analysis has not yet been well established now. The driving force of coarsening is differences in the average energy of different size of the islands. Small islands have higher energy than that of large islands due to high surface ratio against volume. The crystallographic orientation of islands that is related to energy of islands in surface and interface is also a driving force of this phenomenon. If all islands have identical crystallographic orientation, epitaxial growth can be obtained. Schematic diagram of coarsening is shown in Figure 2.8 [20].

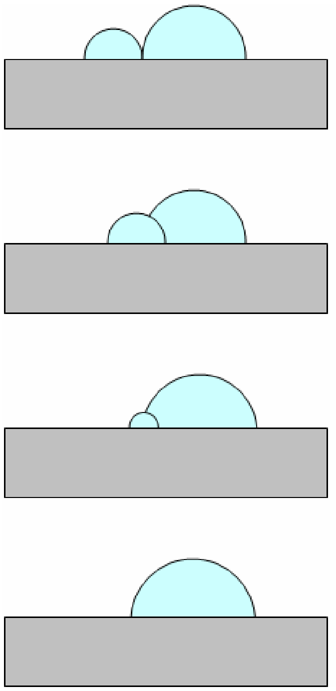

Figure 2.8: Schematic diagram of coarsening. Atoms in both islands exchange with each other through grain boundary motion or surface diffusion

When islands form a network and the channel is filled up completely, continuous film is created at this point called percolation. Percolation means that grains are connected electrically within metal layers on insulting substrate [21]. Thickening occurs after percolation, and grain growth and recrystallization are driven depending on homologous temperature (Ts/Tm). Ts is the substrate temperature during deposition and Tm is the melting temperature of materials. Figure 2.9 summarizes and illustrates film formation, and two types are determined by the homologous temperature [20].

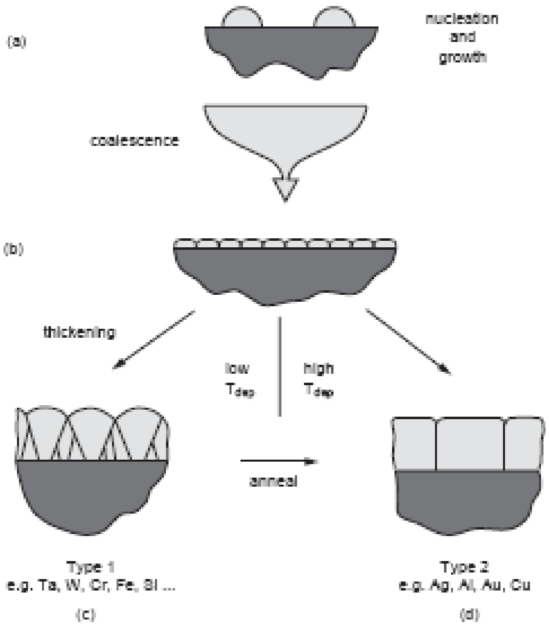

Figure 2.9: Film formation of polycrystalline thin films with their structural evolution

2.3.2 Thermodynamic nucleation and growth

Capillarity theory can be applied to heterogeneous nucleation of a condensed film on the surface of substrate without considering the heterogeneous site on surface. These thermodynamic concepts give us a qualitative model of film formation with factors of critical nucleation size (r*), substrate temperature, and deposition rate, but inaccurate quantitative information. The free energy change in the forming nucleus is shown in Equation 2.3.

$$\Delta G = a_3 r^3 \Delta G_v + a_1 r^2 \gamma_{fv} + a_2 r^2 \gamma_{fs} - a_2 r^2 \gamma_{sv} \qquad (2.3)$$

where a_1r^2 is the curved surface area of nucleus, a_2r^2 is the projected circular area on the substrate, a_3r^3 is the volume, γ_{fv} is film surface energy, γ_{fs} is interface energy, and γ_{sv} is the substrate surface energy. Surface energies are related to Young's Equation 2.4, and these surface energies depend on bonding and structure of surface or interface.

$$\gamma_{sv} = \gamma_{fs} + \gamma_{fv} \cos\theta \tag{2.4}$$

When thermodynamic equilibrium is achieved as $d\Delta G / dr = 0$, critical nucleus size (r*) can be obtained in Equation 2.5.

$$r^* = \frac{-2(a_1\gamma_{fv} + a_2\gamma_{fs} - a_2\gamma_{sv})}{3a_3\Delta G_v} \tag{2.5}$$

Film growth mode is classified in three ways such as Volmer-Weber (island growth) mode, Stranski-Krastranov (layer plus island growth) mode, and Frank-Van Der Merwe (layer by layer) mode in Figure 2.10.

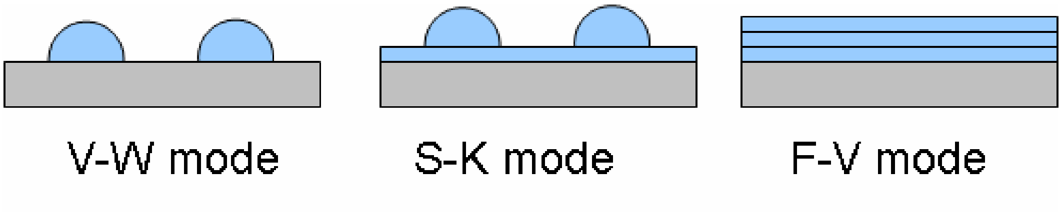

Figure 2.10: Three growth modes. Volmer-Weber mode with θ>0, Frank-Van der merwe mode with θ≈0, and Stranski-Krastanow mode between them.

The capillarity model can qualitatively explain the effect of deposition rate and substrate temperature on nucleation. We assume that deposition rate is proportional to pressure in the condensation process, γ_{sv} goes to zero, and γ_{fv} is same as γ_{fs}. By differentiation of r* and using chain-rule differentiation by plugging in typical values, we can estimate the film growth using Equations 2.6 ~ 2.9.

$$(\partial r^* / \partial T)_{\dot{R}} > 0 \tag{2.6}$$

$$(\partial \Delta G^* / \partial T)_{\dot{R}} > 0 \tag{2.7}$$

$$(\partial r^* / \partial \dot{R})_T < 0 \tag{2.8}$$

$$(\partial \Delta G^* / \partial \dot{R})_T < 0 \tag{2.9}$$

where $\dot{R}$ is evaporation rate and T is substrate temperature. Higher temperature makes islands achieve greater thickness with larger r* and high nucleation barrier ΔG^*. Fast deposition rate R create continuous film with high nucleation rate induced by smaller r* and ΔG^* early. Since this capillarity model is based on macroscopic view on film formation, this continuum concept conflicts with applying small nucleus with few atoms.

2.3.3 Kinetic nucleation and growth

Nucleation rate is introduced by considering time and desorbtion of atoms on surface by kinetic concepts. Nucleation rate $\dot{N}$ (nuclei/cm^2-s) is defined in microscopic view with three terms such as equilibrium concentration of stable nuclei N* (/cm^2), critical area A* (cm^2), and atom impingement rate onto nucleus (/cm^2-s) in Equation 2.10.

$$\dot{N} = N^* \cdot A^* \cdot \omega \tag{2.10}$$

and

$$N^* = n_s e^{-\Delta G^*/kT} \tag{2.11}$$

$$A^* = 2\pi r^* a_0 \sin\theta \tag{2.12}$$

$$\omega = \Phi \tau_s v \tag{2.13}$$

where n_s is total adsorption site density, the exponential term in equation 2.11 is probability of forming critical nucleus, $\Phi = \frac{PN_A}{\sqrt{2\pi MRT}}$ is the number of molecules that strike the surface in unit time and area, $\tau_s = \frac{1}{v} e^{E_{dep}/kT}$ is time on surface, v is vibrational frequency of an adatom on surface, and E_{des} is the energy of desorbing adatoms back into vapor.

Statistical nucleation model was proposed including energy to break apart a critical cluster of i atom clusters into i individual atoms (Ei) in equation 2.14 by Walton and Rhodin [22].

$$\dot{N}_{i^*} = \dot{R} a_0^2 n_0 \left(\frac{\dot{R}}{n_0 v} \right)^{i^*} \exp\left(\frac{(i^* + i)E_{des} - E_s + E_{i^*}}{k_B T} \right) \tag{2.14}$$

where $\dot{N}_{i^*}$ is concentration of critical clusters per unit area, n_0 is total density of adsorption sites on surface, i* and E_i* are constant, and cluster formation energy depends on condition of supersaturation and substrate temperature. In this model, crystallographic information is included and critical size depends on the substrate temperature in microscopic view.

2.3.4 Structure Zone Models (SZMs)

Polycrystalline structure shows a large variety regarding size, morphology, and crystallographic orientation depending on material systems, process parameters, and chamber design. To interpret and generalize microstructure of thin film as a function of deposition parameters, experimental structural models have been proposed with classified several zones that have similar microstructure, named Structure Zone Model (SZM). After first being proposed by Movchan et al. [23], Thornton [24, 25] and Messier et al. [26] proposed SZMs for sputter deposition films and ion-assisted deposition films with RF cathode respectively. Also, SZM for evaporation deposition technique was modeled by Grovenor et al. [27]. Moreover, many revised SZMs have been suggested from above representative SZMs to correct divergence of difference systems, because various film structures are induced from versatile variables of process. In spite of the impreciseness of SZMs, they give us much information about microstructure.

2.3.4.1 SZM for evaporated films

Grovenor et al. proposed a structure zone model for metallic film deposited by the e-beam evaporation system [27]. SZM model was revised at low temperature region (less 0.2 homologous temperature) from Movchans and Demehishin’s and Thornton’s SZM, and built up based on experimental results of metallic film deposited on amorphous substrate for thin (100nm) films and polycrystalline substrate for thick (9~14) films in Figure 2.11.

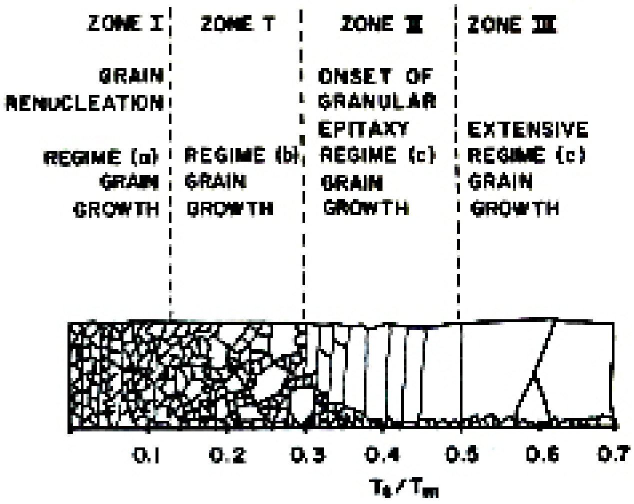

Figure 2.11: Grovenor's structure Zone Model [27]

Very fine equiaxed grains are formed at Zone I with grain renucleations in thin and thick films. Although it is proposed that deposited atoms stick to the surface they land by restricted mobility due to low temperature, this granular and small grains are not well understood by current mechanisms [23]. As limited mobility of grain boundary in Zone I is released in Zone T and Π, grain is getting larger and porosity is decreased by onset of surface diffusion. Bimodal grain size contribution appeared in Zone T with abnormal grain growth mechanism [20]. Columnar structures with uniform grain size distribution are produced in Zone Π by surface recrystallization and bulk diffusion. Granular epitaxy structure has smaller dimension of grain size (d) than thickness (t) as d/t<1, but d/t goes head to unity as temperature increases. At the boundary of Zone П and Ш, wider and more uniform columnar structure is produced to ultimately exceed unity of d/t.

2.3.4.2 SZM for sputtered films

Thornton developed the Structure Zone Model of sputter-deposited thin film based on homologous temperature (Ts/Tm) and process gas pressure in Figure 2.12. Messier et al., who developed SZM with ceramic films by RF sputtering, suggested that Thornton's SZM can be applied to thin film that is deposited by wide method of vapor deposition and most of metallic and ceramic materials [28, 29].

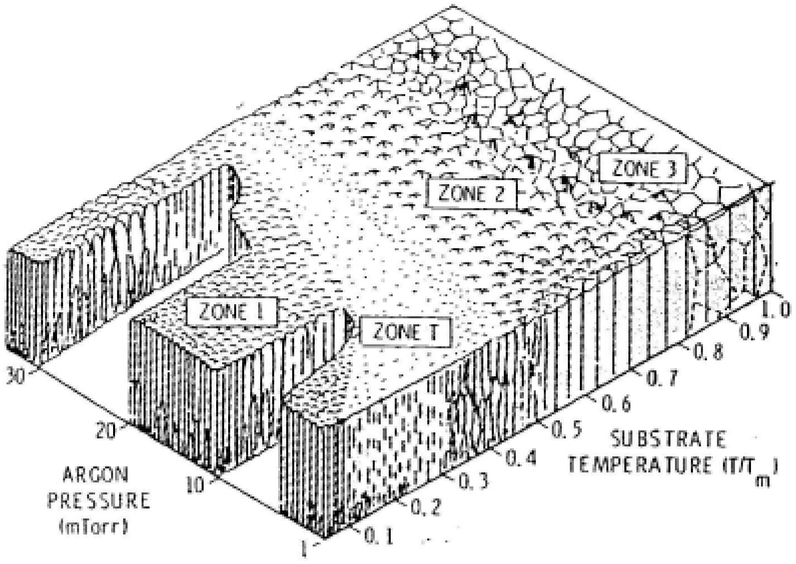

Figure 2.12: Thornton's Structure Zone Model showing the influence of substrate temperature and process pressure on metallic thin films [24]

Since the density of inert gas induces collision with sputtered atoms, surface diffusion is limited by reduced kinetic energy of adatoms and they arrive at substrate in random directions resulting in shadowing effect. Pressure effect on microstructure is not large on films deposited at high homologous temperature, but the boundary of zones shifts to higher homologous temperature with pressure at relatively low homologous temperature as shown in Figure 2.12. Thorton et al. also supposed that high absorption of Ar gas into film at high processing pressure suppresses the diffusion of atoms. Both cases create the same result in low diffusivity at high chamber pressure condition.

SZM is classified in four regions dependent on the microstructure of cross-sectional view such as zone 1, zone T, zone 2, and zone 3. Columnar grain with small grain size is produced at Zone 1, and grain size gets bigger as temperature increases. Restricted mobility of atoms by low temperature creates voided boundaries. Since high deposition rates suppress the mobility of atoms, voids can be reduced with low deposition rates.

Zone T is transition zone between zone 1 and zone 2. Dense fibrous structure is formed by relatively increasing temperature, and surface morphology is smooth with high reflection. Faucet rich columnar structure is produced at zone 2 with large grain size. Equiaxed grains are formed at zone 3 with its high mobility of diffusion, and groovy grain boundaries are created.

2.4 Film stress

Stress in film is a distinctive issue on their applications. Large stress induces defects such as voids and hillocks so that they degrade film properties in most ways. Films storing too much stress can bend their parent device or film might peel off. Stress on film is either tensile or compressive, and their momentum between substrate bends substrate concave upward by tensile stress, and convex downward by compressive stress to compensate for momentum. Figure 2.13 shows events loaded by both conditions.

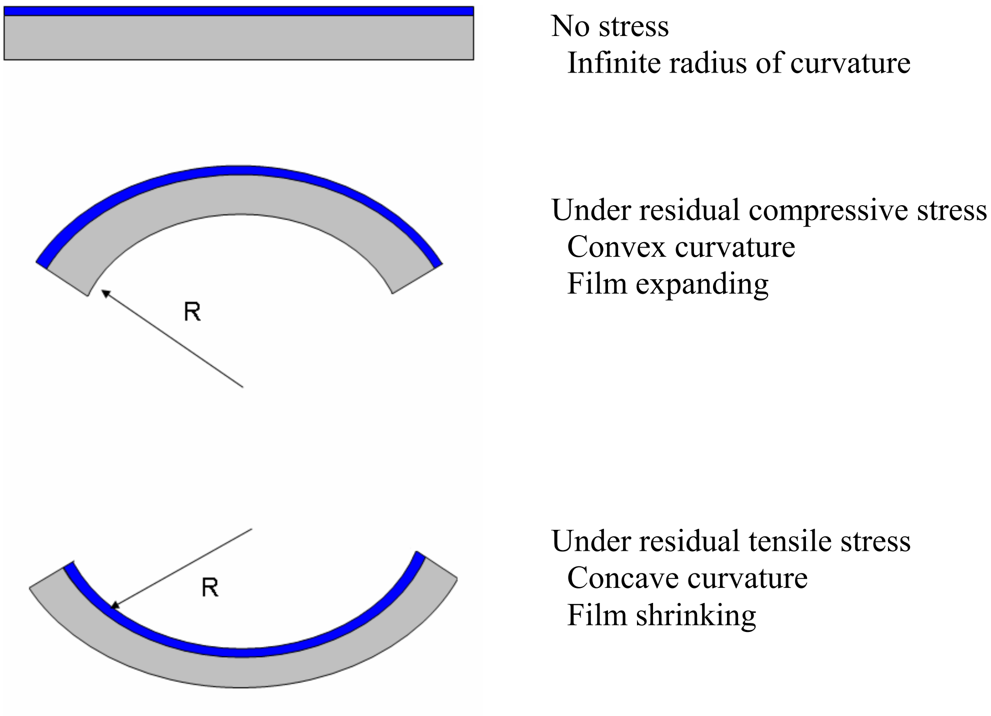

Figure 2.13 Stresses on film

Most films are under tensile or compressive stress in their use, and their origin classified by thermal, external, and intrinsic. Thermal stress is presented by different thermal expansion coefficients between film and substrate in applied temperature. Thermal stress is given in uniaxial approximation as

$$\sigma_{Thermal} = E_f(\alpha_f - \alpha_s)(T_s - T_A) \tag{2.15}$$

where E_f is Young's modulus, α_f and α_s are thermal expansion coefficients of film and substrate respectively, T_s is substrate temperature during deposition, and T_A is the temperature during measurement.

External stress is caused from interaction between film and the environment such as humidity. Intrinsic stress is mainly due to crystallographic mismatch between the substrate and film itself during deposition at low homologous temperature. On the contrary, intrinsic stress as well as thermal stress should be considered on microstructure built up when condensation of thin film is performed at deposition. Intrinsic stress is caused from some components that induce tensile or compressive stress, so that a deeper study of stress generated at stages of film growth is required to understand the final microstructure evolution of films.

The relationship between temperature and stress can be approximately understood by Thornton's plot in Figure 2.14 [30]

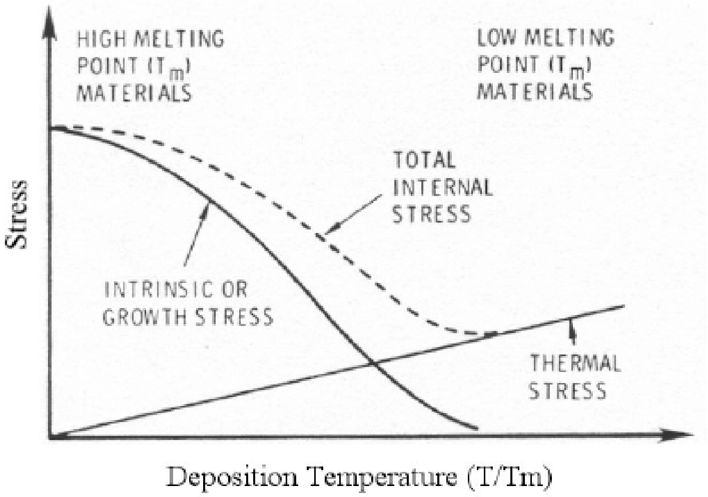

Figure 2.14: Relationship between thermal and intrinsic stress as homologous temperature

2.4.1 Intrinsic stress during deposition

It is not in thermodynamic equilibrium, so that most film growth strongly controlled by kinetic energy. Far from perfect single crystals, films have many types of defects that are sources of stress. Stress in film are contributed by such factors as

1. Small angle of grain boundary
2. Recrystallization
3. Lattice expansion up to percolation
4. Capillarity stress
5. Impurities

It is well known that grain boundaries are a possible source of intrinsic source in films. In polycrystalline films, grains are randomly oriented with a high concentration of small angle grain boundaries between themselves. Low density in grain boundaries create gaps between grains, and inter-atomic forces between adjacent grains tend to close this gap [31]. Grains are strained by a neighboring one, and small angle boundary effect produces tensile stress in film. Small grain size creates large grain boundary areas, and they increase tensile stress (σ_{gb}) in film.

$$\sigma_{gb} = \frac{E_s}{1-v_s}\frac{d}{D} \tag{2.16}$$

where d is the average atomic relaxation distance, D is grain size, E_s is Young's modulus, and v_s is poison ratio.

Compressive strain between domain walls is produced by emmerging favorable bonding at domain walls filling up the gap between islands [32]. This compressive stress is applied to epitaxial Volmer-Weber mode, and atoms at the gap between islands result in crystallographic displacement from perfectly arranged orientation.

Recrystallization of film is dominated by diffusion of atoms, and it produces larger grain size with increased densification. Recrystallization occurs during and after deposition, and leads to the development of tensile stress due to eliminated defects such as grain boundaries and voids [33]. Chaudhari et al. [34] quantified recrystallization stress with grain size in equation 2.17.

$$\sigma_{recr} = \frac{2E}{1-v} \Delta v_{ex} \left(\frac{1}{D_0} - \frac{1}{D} \right) \tag{2.17}$$

where D_0 is initial grain size, D is final grain size, and Δv_{ex} is volume change between grain boundary area and that of a single crystal.

The lattice parameter of small islands on the surface is smaller than that of bulk in equilibrium of condensation process of films [35, 36]. As islands grow, the lattice parameter of a small particle can expand and reach to that of bulk. In reality, this expansion can not reach the inherent lattice parameter of material, because particles are partially anchored by the surface of substrate. Adhesion between film and substrate at the island growth stage produces compressive strain in each island, and compressive stress distributed on films before forming continuity [37]. If adhesion is not strong enough to stand under compressive stress, it can be relax due to island growth [38]. After islands grow and percolate with continuous film, relaxation by island gliding does not work any longer. Compressive stress is stored in continuous films, and reslts from capillarity stress [39].

Impurities in film restrict surface diffusivity by positioning in interstitial sites or grain boundaries [40]. These impurities are induced by very reactive components in the chamber with very low partial pressure such as O_2, H_2O, and so on.

2.4.2 Stress in sputtered films

Evaporated films are relatively easier to generalize the film stress than that of sputtered films due to its simple mechanism of deposition. It is well known that film formation is very dependent on diffusivity of atoms, and microstructure that results from the atom's diffusivity is premier aspect to characterize film properties even in stress. Hence, homologous temperature of substrate surface is strong variable to determine residual stress in film in evaporation deposition systems. Figure 2.15 shows the relationship between stress and process temperature in thickness of silver films in Volmer-Weber growth mode [41].

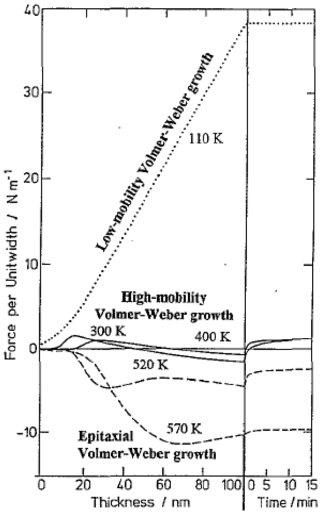

Figure 2.15: Stress vs. thickness of silver films deposited by evaporation system onto mica (001) with varying temperature.

Sputtered films produce complex stress distribution depending on process parameter due to complicated deposition mechanism with many variables. Windschmann [42] suggested equation 2.18 based on volumetric distortion of sputtered films in tensile .

$$\sigma = \frac{k\Phi\sqrt{E}MY}{(1-\nu)\rho} \tag{2.18}$$

where Φ and E are the ion flux and energy, respectively, M is mass of atoms, Y is Young's modulus, v is poison ratio, ρ is density of film, and k is a constant. As the equation indicates, film stress varies with process parameter. For example, gas pressure changes ion energy by collisions, and compressive stress is dominant at low gas pressure by atomic peening mechanism. Figure 2.16 shows the stress variation of metal films as process pressure [43], and the general effect of parameters on stress of sputtered film are listed in Table 2.3 [44] .

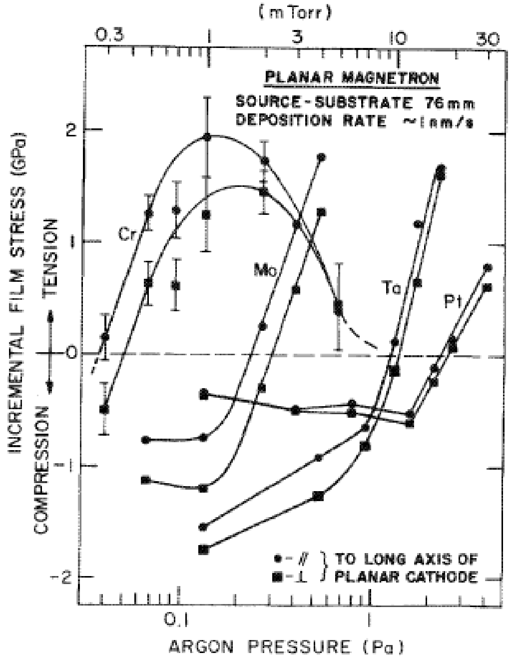

Figure 2.16: Biaxial internal stress depends on argon pressure in chamber for Cr, Mo, Ta, and Pt metallic films sputtered by planar magnetron source onto glass [43]

Table 2.3: Effects of sputtering process parameters on film stress at low homologous temperature[44]

Compressive	Variable	Tensile
Low	Gas pressure	High
Negative	Substrate bias	Positive
Low	Gas atomic mass	High
High	Target atomic mass	Low
Normal	Angle of deposition	Oblique
Cylindrical	Target shape	Planar

2.4.2 Stress characterization

The techniques for measuring internal stress in films are classified by measuring deflection or curvature of substrate, and using x-ray diffraction to determine elastic strains. The x-ray method has a somewhat large error range with high "smallest detectable stress," but it is useful to determine the type of stress involved whether compressive or tensile. X-ray measurement uses slight change of interplanar spacing in crystal plane in equation 2.19. If film is under tensile stress, interplanar spacing in normal plane to substrate will be contracted.

$$\sigma_f = -\frac{Y(a - a_o)}{2\nu a_o} \tag{2.19}$$

When Y is Young's modulus, ν is poison ratio, a is lattice spacing, a_o is unstressed bulk lattice in z direction.

CHAPTER 3

EXPERIMENTAL SETUP AND TECHNIQUES

This chapter consists of three sections. In the first section, substrate preparation for film deposition in the thesis is explained. Three kinds of substrate, such as SiO_2, glass, and photodiode, were used for each purpose. A sputtering system was used with a various and wide range of process parameters. Commercialized sputtering system modified to cool down substrate temperature is introduced in the second section. In the last section, film characterization such as thickness measurement, surface morphology analyzing, reflectance test, and electrical conductivity test is described.

3.1 Substrate preparation

Amorphous SiO_2 substrate was grown on Si wafer by thermal atmospheric-pressure chemical vapor deposition (APCVD). Uniform SiO_2 was grown on a 75 mm diameter Si wafer in O_2 environment for 8 hours at 1100 C in a furnace, and its thickness is 3000 Å. Before oxide growth, Si wafer was cleaned by a diluted HF dip (20:1, H_2O:HF) to remove a thin oxide strip. SiO_2 substrate was used to analyze the surface morphology of deposited films, and measure sheet resistance to prevent leakage current though substrate.

Slide Glass substrate and photodiode were prepared to measure reflectance. The glass was cleaned with acetone to reduce the effect of impurity on film growth. Photodiode is a commercialized one manufactured by International Radiation Detectors Inc. (IRD). This device uses silicon p-n junction diode for applications in ranges from extreme ultraviolet to soft x-ray. Electron-hole pairs are created by exposing photons of energy greater than 1.12 eV (wavelength less than 1100 nm). The surface of diode was coated by SiO_2, and its schematic structure is shown in Figure 3.1

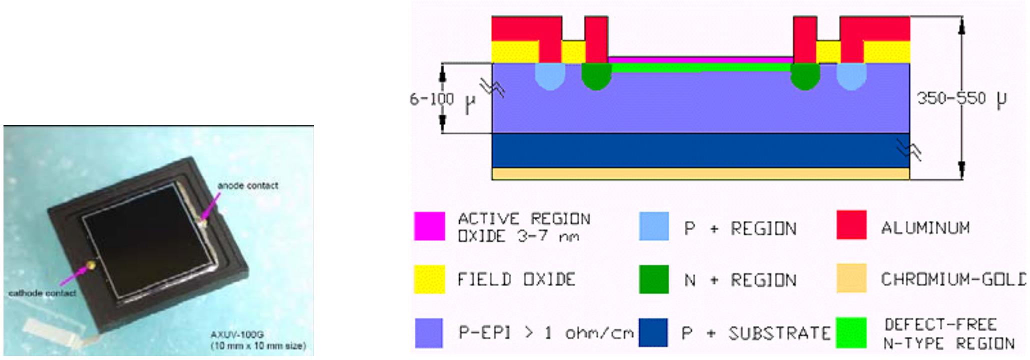

Figure 3.1: AXUV-100G photodiode & structure of photodiode manufactured by IRD Inc..

3.2 Sputtering deposition

A DC magnetron sputter deposition system, made by Denton Vacuum Inc., was used to deposit metallic films. A high magnetic sputter gun enables a high rate of deposition in low pressure, and has a 30 degree angle to substrate for capability of co-sputtering that can deposit compound materials. It has two kinds of substrate such as rotating and hold substrate. The first one can rotate from 0 to 40 rpm speed during deposition, and can be heated by a heat element installed under substrate. The distance between the center of the cathode to the substrate is 100mm, and substrate can be heated to 350^{o}C in calibrated temperature. Ar is used for working gas with range of flow rate in 5 ~ 100 sccm, and corresponded process pressure can be varied from 1 mTorr to 24 mTorr with controlling throttle valve manually. Cathode power can be applied up to 600 W. A schematic illustration of Denton sputtering system is shown in Figure 3.2

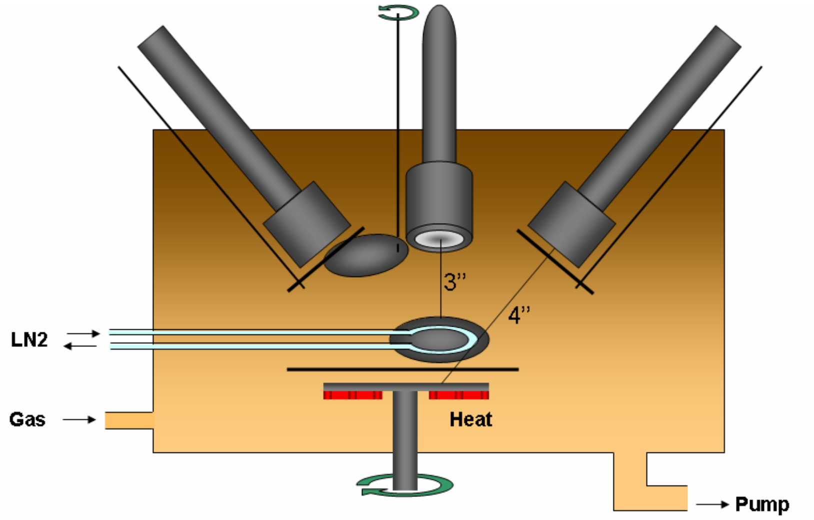

Figure 3.2: sputtering system

The cooling stage was added on sputtering system in normal angle to the cathode. After supplying liquid nitrogen through the pipe for 30 minutes, the SiO_2 piece on substrate could be cooled down to -110 C. Figure 3.3 is temperature calibration of cooled substrate.

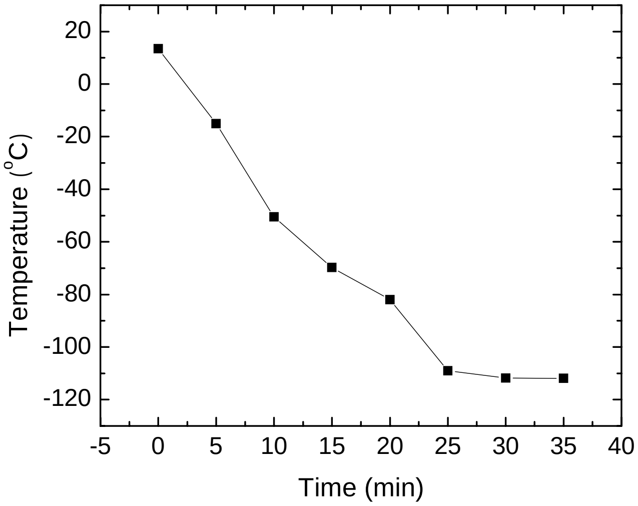

Figure 3.3: Temperature calibration of LN_2 cooled substrate

Table 3.1: Available range of process parameter of sputtering system

Parameters	Range
Power	< 600 W in DC and RF
Gas flow	5 ~ 100 sccm
Pressure	1 ~ 24 mTorr
Temperature	-110 ~ 350 C
Base pressure	$5x10^{-7}$ Torr

The available process parameters and their ranges in Denton sputtering system is summarized in Table 3.1.

The target is a cylinder type with a 75 mm diameter. To prevent impurity effect on deposited film, highly pure Ar (99.9999% purity) and pure targets (more than 99.999%, indium target) were used. A high vacuum is obtained by pumping out through a turbo pump.

Pre-sputtering was performed before deposition to clean up the target surface of oxide or nitride, and power was stabilized during pre-sputtering. The Denton sputtering system has two kinds of shutters: heat and cathode shutter. The heat shutter is located above the substrate to prevent heat transfer from substrate to cathode. The cathode shutter is closed to the cathode during pre-sputtering with restricting plasma near the cathode surface, and opened when deposition is initiated.

As power increases, the target temperature can be raised up too high to withstand its high temperature. Since indium has a very low melting temperature of 156^{o}C, sputtering power is limited below 150 W.

3.3 Film characterization

3.3.1 Film thickness

An attempt was made to measure indium film thickness using profilometer. Vacuum tape attached to glass during deposition, and it was removed after deposition to make step on films. Since the stylus moving left a trace on the surface of indium films due to its softness, the results of the profilometer method made many errors enable to determine exact thickness. Scanning electron microscopy (SEM) was used to measure thickness of indium thin film. A cross-section view of films is scanned in Figure 3.4.

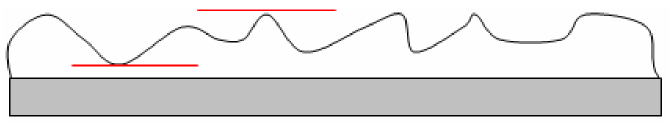

Figure 3.4: Thickness measurement by SEM

Since surface morphology of indium thin film is very rough, thickness is obtained by taking the average between the highest and lowest thickness in SEM pictures. More than three pictures of the SEM cross-section view were sampled and averaged out, and reported in the thin study.

3.3.2 Surface morphology analysis

Scanning electron microscopy (SEM) and atomic force microscopy (AFM) were used to analyze surface morphology such as grain, grain boundary, and roughness. SEM, manufactured by JEOL, gives enough high resolution images to define microstructure and film growth mode. The non-contact mode of AFM was used to prevent making marks on the film and making error. Tunneling current depending on morphology of film induces movement of the cantilever stylus up and down. Laser reflects on the photodiode at the end of the cantilever, and the intensity variation of the reflected beam as the surface morphology creates an image with amplified electrical signal from photodiode. A schematic illustration is shown in Figure 3.5.

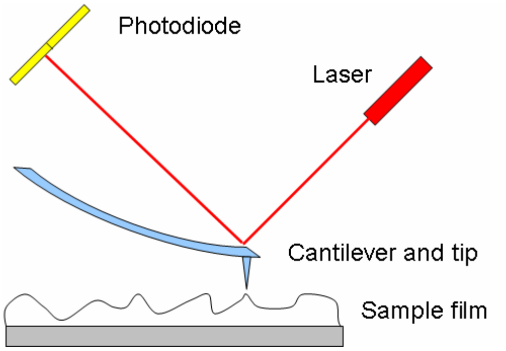

Figure 3.5: Atomic force microscope (AFM)

Energy dispersive spectroscopy (EDS) is used to investigate impurity composition in pure metallic films.

3.3.3 XRD analysis

X-ray diffraction (XRD) was performed for crystallinity and stress analysis of thin films using CuKα radiation and a scanning speed of 0.05^{o} per second. Films on silicon pieces were used, and correction of peak shift by tilted sample loading was performed to determine stress on films. Preferred orientation is indicated by intensity of a diffraction pattern, and strain induced by stress can be determined by peak positions after correction of peak shift by other factors.

3.3.4 Sheet resistance

Film resistivity was measured by a 4 point probe, manufactured by Lucas Labs, and a Keithley 2400 Source Meter Current Meter. A constant current is applied to the sample by two outer probes, and voltage is measured by other probes. Thin films have much a smaller dimension of thickness (t) than spacing of probes (s), and resistivity is given by

$$\rho = 2\pi sV / I \ \mu\Omega - cm^2 \tag{3.1}$$

and sheet resistance as

$$R_s = \rho / t = (\pi t / \ln 2) V / I \ \mu\Omega - cm \tag{3.2}$$

CHAPTER 4

RESULTS AND DISCUSSIONS

This section consists of three parts. In the first part, microstructure evolutions are shown as controlling process parameters based on kinetic and thermodynamic considerations. Energy and number of adatoms are controlled by power, pressure, and distance between cathode and substrate. Microstructures of indium films are modified dramatically by applying cryogenic substrate temperature. In the second part, optical and electrical properties of films are supplementarily characterized to obtain more quantified information of films. In the last section, the Structure Zone Model is revised with its surface roughness for low melting temperature material.

4.1 Thin film growth of indium system

Indium films were deposited at moderate pressure with consideration to chamber design. While sputtering power was restricted during the process to prevent melting of indium target due to its low melting temperature, the substrate mostly maintained at room temperature due to the short processing time. Although the substrate temperature is room temperature, the homologous temperature Ts/Tm is very high - “high-mobility material.” Table 4.1 shows process parameters, and the substrate is located on a rotating plate with angled cathode to plate.

Table 4.1. Process parameters of indium sputtering deposition

Process parameters	Contents
Power	DC 100W
Pressure	5 mTorr
Ar gas flow	25 sccm
Substrate temperature	Room temperature ± 5 ^{o}C
Homologous Temperature (Ts / Tm)	0.70
Base pressure	5x10^{-7} Torr
Deposition rate	10 Å/sec

Indium films were deposited on silicon dioxide by DC sputtering under the same conditions except time, and then its film formation was scanned from nucleation to thickening by a scanning electron microscope (SEM) in Figure 4.1.

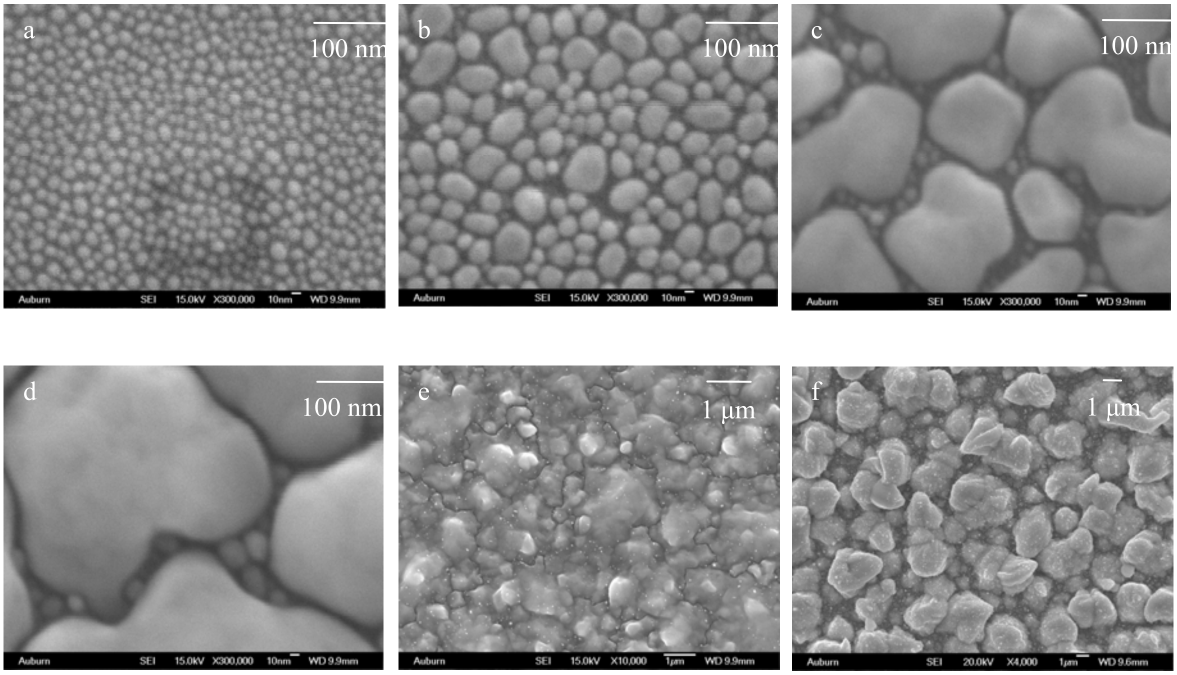

Figure 4.1: Structural evolution of indium film at room temperature; films are sputtered with 100W cathode power, 5 mTorr pressure, for a) 6 sec, b) 11sec, c) 26 sec, d) 50 sec, e) 200 sec, and f) 1000 sec.

Film formation show strong Volmer-Weber (V-W) growth mode. In the initial stage, a large number of nucleation islands were generated on SiO2 substrate layer (see Figure 4.1-a). As deposition is continued, islands are enlarged by additional impinging adatoms and coalescence among island increases the size of each until a percolation network is attained. Also, small and new nucleated island were found between large islands (see Figure 4.1-b,c,and d). Percolation means that grains are connected electrically within the metal layer on insulating substrate, and percolation was achieved around 70~80 nm thickness in indium system. After forming continuous film, grain size was continuously larger with recrystallization. Note that very rough surface morphology was shown and increasingly worse (see Figure 4.1-e and f) with shaping gibbous or faucet. These abnormal shapes were distributed on the middle of grains of entire surface.

Indium, “high mobility material”, has very high diffusivity at room temperature due to its low melting temperature. High diffusivity makes atoms migrate onto the high energetic surface site and release the elastic energy of films, and film stress would be released. If time term is considered in kinetic concepts, it is unavoidable to generate internal stress in itself. The evaluated stress was characterized in evaporated thin film by Abermann et al. and reviewed by R. Koch. The smaller lattice parameter of thin film, constrained by adhesion to the substrate layer, tends to expand and reach to that of bulk materials during the coalescence stage in high mobility materials. This gliding of islands induces compressive stress in each grain when percolation restricts the gliding and tensile stress due to small angle grain boundary before percolation switch to compressive stress in whole film. The relaxation of compressive stress generated by the grain coalescent process creates the appearance of gibbous faucets. Also, it seems that shadowing effect of sputter system enhances the roughness of the film. Aluminum has a low melting temperature as 660K has been sputtered at the same homologous temperature (Ts/Tm = 0.7); those films are shown in Figure 4.2 comparing indium film. They also had very rough surface morphology, and large and contributed faucets or agglomeration. It seems that the shadow effect of sputtering system also enhanced this rough surface up in thick (1 μm) films.

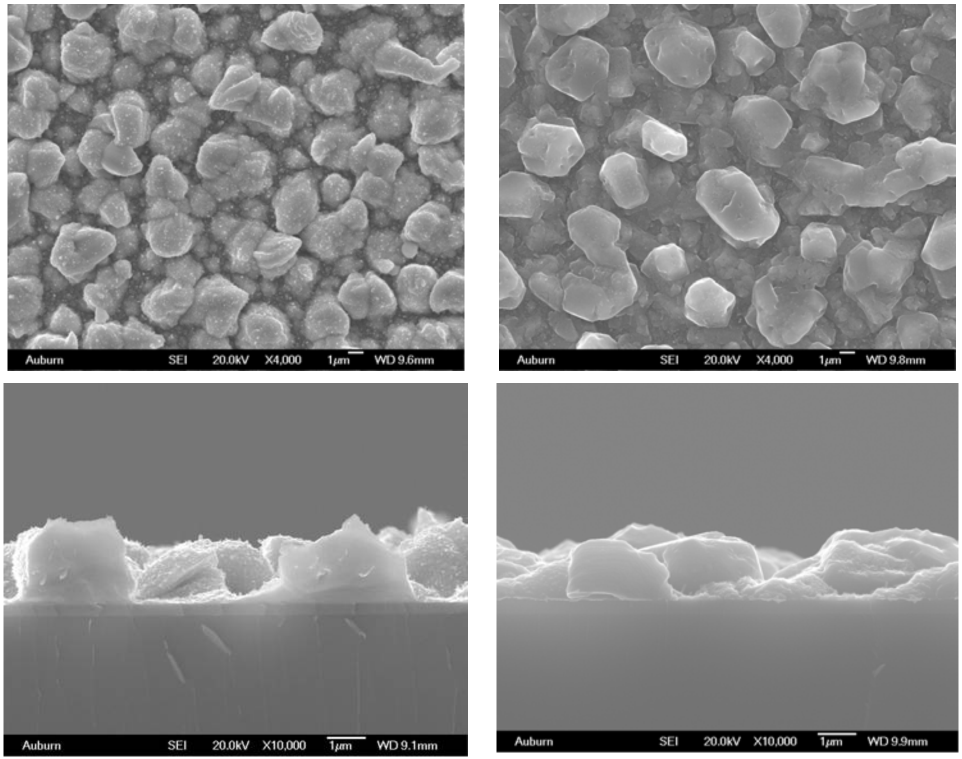

(a) (b)

Figure 4.2: Morphology of 1 μm films in high mobility material system. a) indium (273K), b) aluminum (523K) films were sputtered at the same homologous temperature (Ts/Tm = 0.7).

Compressive stress generation is related to the diffusivity of atoms during film formation. It can, therefore, be said that diffusion controls of adatoms changes the microstructure in major, although internal stress is one of pointed factors of microstructure evolution. Although TEM analysis gives us abundant information about microstructure and stress, XRD is an available technique that allows characterization of stress in qualitative and quantitative ways. XRD characterizing will be shown later.

4.2 Microstructure evolution against process parameters

Microstructure was evolved by changing process parameters of sputtering deposition based on knowledge of thermodynamic and kinetic concepts. Deposition conditions were explored to control three factors: (1) energy of impinging adatoms, (2) substrate temperature, and (3) deposition rate. They are major considerations very relative to surface and bulk diffusion in the film formation mechanism. Since film formation is usually interpreted by solid state condensation of adatoms in PVD method, cathodic power and processing pressure were adjusted to control plasma that supervises energy of impinging adatoms. Deposition rate, "ion flux", was controlled by adjusting the distance between cathode and substrate, and substrate temperature was cryogenically cooled down by liquid nitrogen. Heat treatment was performed on deposited film, and the annealing effect after deposition was compared with as-deposited film at high homologous temperature in view of microstructure modification in thermodynamics. Low diffusivity of atoms on surface and bulk of film restrict the enlarging island, and then the capillary force that creates compressive stress on film will be diminished. Technically, rough surface and distorted crystallography of indium sputtered film is caused from high mobility of its adatoms. In other words, a smooth surface can be obtained by lowering its diffusivity by any means.

4.2.1 Deposition rate (ion flux)

High deposition rate or a large number of impinging atoms rate makes film growth mechanism nucleation dominant. Since increasing power was limited to prevent melting the target, the distance between target and substrate was shortened from 100mm to 75mm. The deposition rate increased from 10 Å/sec to 25 Å/sec at room temperature. The film with the smoother surface and smaller grain size was generated by deposited indium film at a higher deposition rate, and rough and large-grained indium film that deposited at a low deposition rate was compared through SEM in Figure 4.3.

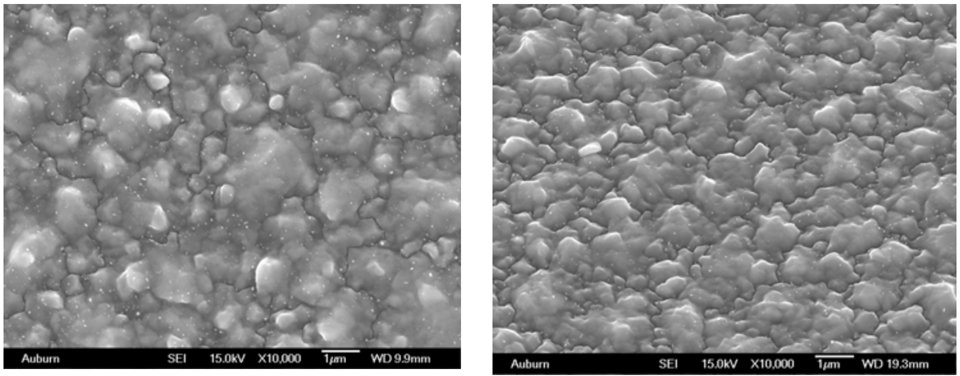

(a) (b)

Figure 4.3: Surface morphology of indium films that deposited with the same conditions except time and distance between target and substrate as a) 100 mm (200sec), and b) 75 mm (80sec). Each film has 2000 Å thickness.

Since the shape of grain was irregular, the value of grain size could hardly be estimated. But, it can be easily intuited that film with a high deposition rate has smaller grain with more grain boundary regions. Nucleation seems to be activated by increasing the number of impinging atoms in Equation 2.10, and the nucleation dominant process creates more fine grains by restricting diffusion of atoms that landed on films from vapor.

Faucets existed on entire film regions after increasing deposition rate, but their height was reduced based from data from APM analysis with non-contact mode in Figure 4.4.

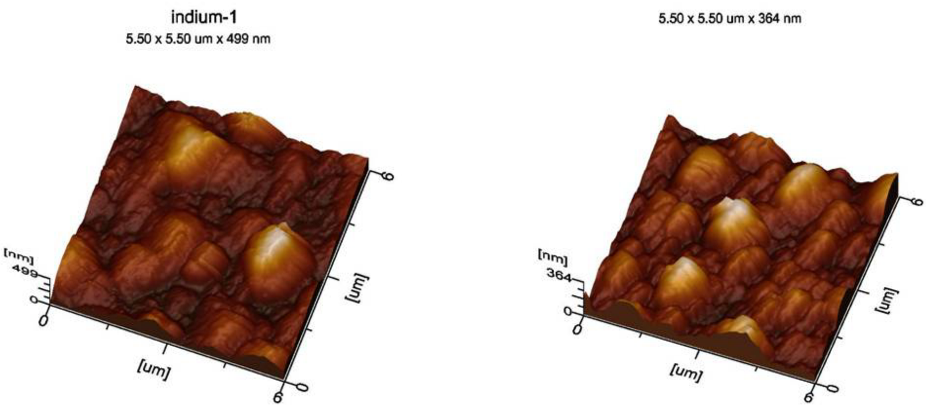

(a) (b)

Figure 4.4: Surface scanned by APM for two indium films: a) low deposition rate, RMS 90.1 nm, and b) high deposition rate, RMS= 67.7 nm

If the deposition rate is short, diffusing atoms on the film's surface does not have enough time to find and move into position on high surface energy. Although the deposition rate is not directly related to the diffusion of atoms, the short deposition rate can restrict the normal film formation such as nucleation, coalescence, and recrystallization. The effect of high deposition rate is similar to that of temperature that can effectively control diffusion of atoms in Arrhenius relationship. It is proven that deposition rate and temperature has a linear relationship in deciding microstructure between monocrystals and polycrystals in Figure 4.5.

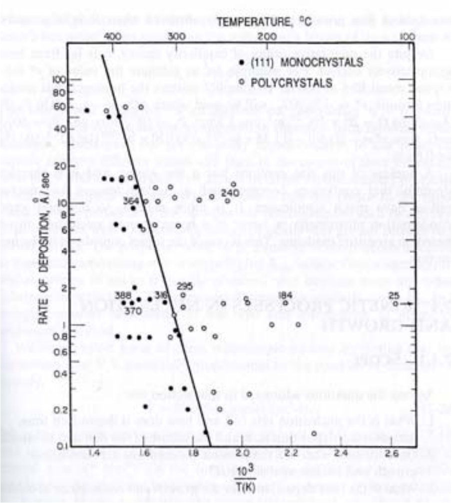

Figure 4.5 Microstructure depends on deposition rate and substrate temperature [45]

4.2.2 Energy of impinging adatoms

Diffusion on the surface of the film is interpreted by energy in thermodynamic and kinetic consideration. From Equations 2.10 and Equation 2.14, nucleation rate and diffusion of adatoms are closely related to the desorption and diffusion energy barrier in exponential terms. The energy of impinging adatoms was changed by controlling process pressure as 5 mTorr with 25 sccm, 9.8 mTorr with 50 sccm, and 14 mTorr with 75 sccm. Argon was used for ionized gas to generate plasma, and flow rate is reported. It is no meaningless quantify the energy of adatoms when they have arrived at the surface of the sample, because every chamber has its own characteristic with gas flow geometry depending on size and shape. It can be said that the energy of adatoms decreases with pressure at which the number of collisions between target and gas molecules are decided. The morphology of indium surface was characterized by SEM, and it is in Figure 4.6. Process parameters are on Table 4.2.

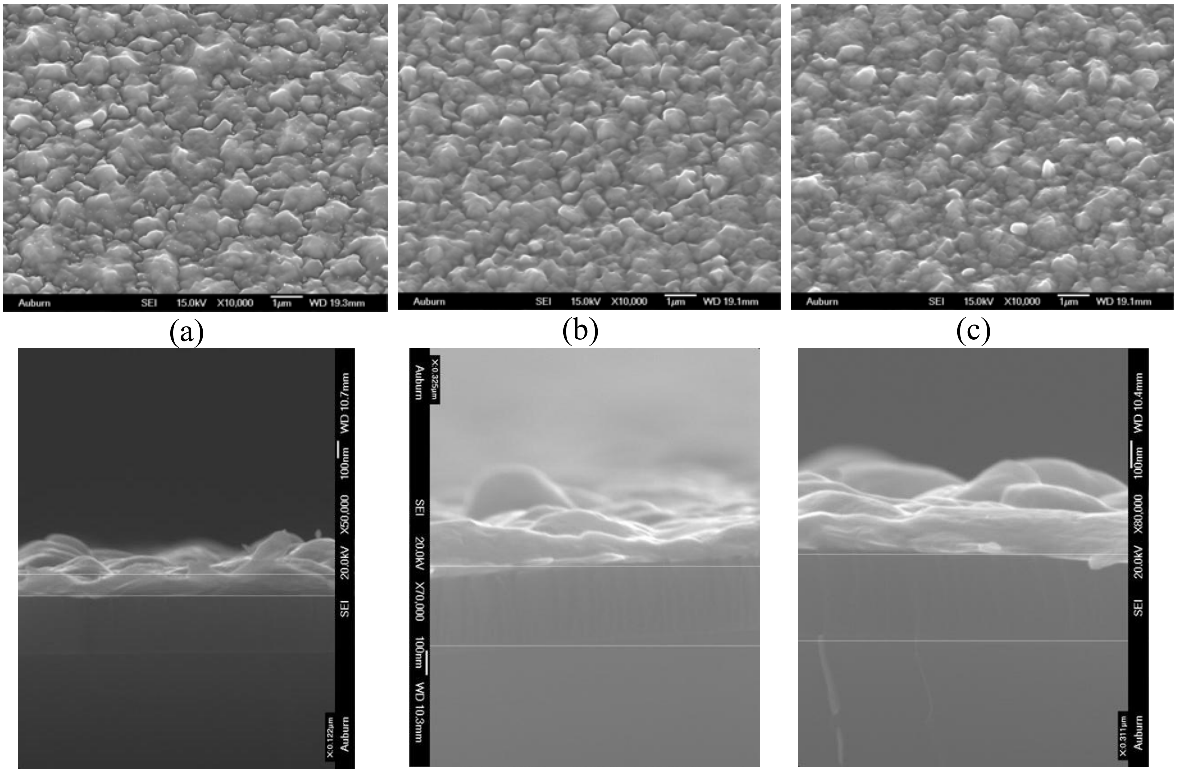

(a) (b) (c)

(a) (b) (c)

Figure 4.6: SEM analysis of indium films sputtered at different pressure: a) 5 mTorr, b) 9.8 mTorr, and c) 14 mTorr.

Table 4.2. Process parameter of films in Figure 4.6

Process parameters	Contents
Power	100W DC
Time	80 sec
Distance between target and substrate	75 mm
Thickness	1500 ~ 2000 Å thickness
Substrate Temperature	Room temperature
Base pressure	5x10^{-7} Torr

Deposition rates of each film are very similar to each others due to the high deposition rate in close distance between target and substrate. Thicknesses of films were measured by the cross section view of SEM pictures, and averaged between the highest and lowest level of films. SEM analysis of surface morphology did not make a big difference in the microstructure. Each film was scanned by APM, and smoother surface was made by increasing process pressure, and shown in Figure 4.7.

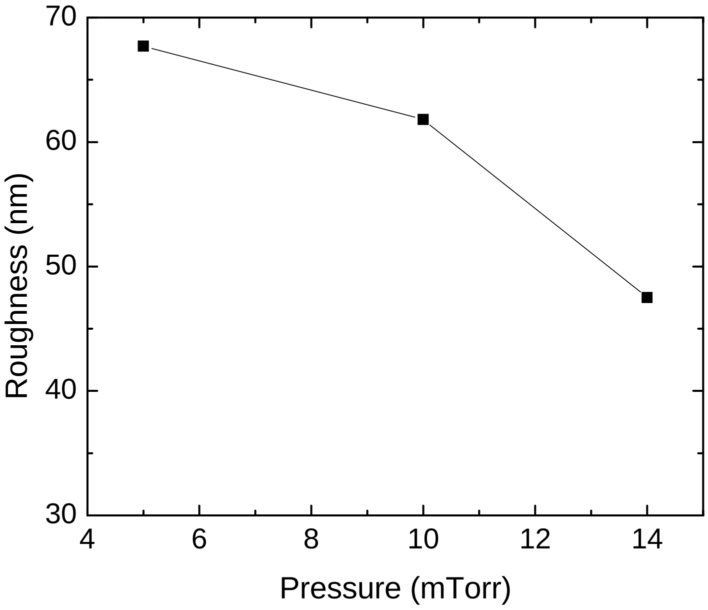

Figure 4.7: Process pressure vs. roughness

Adatoms passed through a high concentration of Ar produced a larger number of collisions that made them lose energy from diffusion and create an oblique angle of impinging. Tensile stress is generated by less momentum bombardments; this is adverse effect to generate faucets by compressive stress. It makes good agreement that high pressure sputtering created smoother morphology. In contrast, sputtering at low pressure has a long mean free path, and the films showed rough surface with high faucets.

4.2.3 Substrate temperature cooled by cryogenics

The substrate has been cooled down to restrain surface and bulk diffusion of atoms during film growth by applying liquid nitrogen. Before starting deposition, liquid nitrogen has flowed through the pipes installed under the substrate for 30 min. The temperature on the surface of silicon wafer located on the substrate was calibrated by thermocouple under the vacuum, and the lowest temperature was noted at 163K, and temperature was saturated at that point. Liquid nitrogen has been continuously flowed during sputtering, and warmed up the substrate by supplying air after deposition. Substrate temperature reached room temperature 30 min after starting warming up, and water absorption and intensive oxidation of film were avoided.

Indium was deposited at 163K with 0.38 homologous temperature (Ts/Tm).100W (DC) power, 75 sccm Ar flow, 14 mTorr pressure, and 5x10-6 Torr base pressure were applied as deposition conditions. Its SEM images are shown in Figure 4.8.

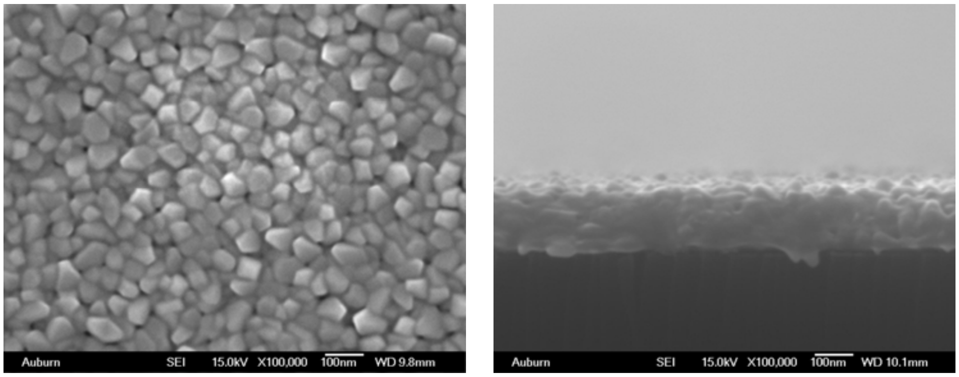

(a) (b)

Figure 4.8: Indium film sputtered at 163 K: a) top view and b) cross section view.

Fine grain (average less than 100nm) was formed in the entire film due to the low surface diffusion. After admolecules were landed on the surface, nucleation and coarsening occurred. Then, recrystallization and coarsening were repeated on the grain that has already grown with high probability due to low surface diffusivity. In the cross section view, granular structure was shown in a vertical direction. This granular structure was proposed by Grovenor et al. in the range of less than 0.2 homologous temperature (see in figure 4.9). Zone 1 was shifted to the homologous temperature range of zone 2 in indium system.

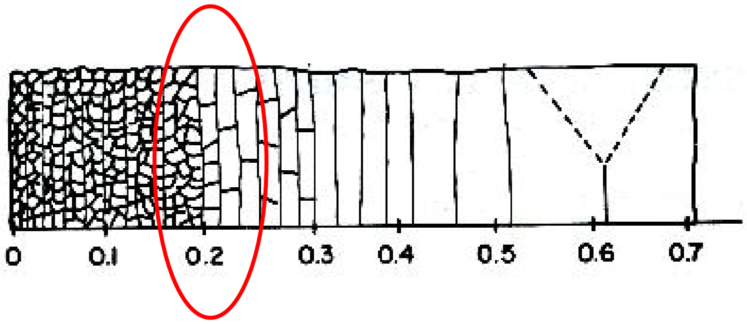

Figure 4.9: Grovenor's SZM

4.2.4 EDS analysis

Granular structure was shifted to higher Ts/Tm zone in Structure Zone Model. It is suspected that the extrinsic defects, such as the impurity of Ar traps and oxidation, causes granular structure with abundant renucleation, because those defects can play a role in the nucleus with high surface energy. In this experiment, we used high vacuum chamber ($5x10^{-7}$) and high purity of Ar gas and target to prevent a contamination during fabrication. EDS analysis was performed to explore impurities on film, and the results are shown in Figure 4.10.

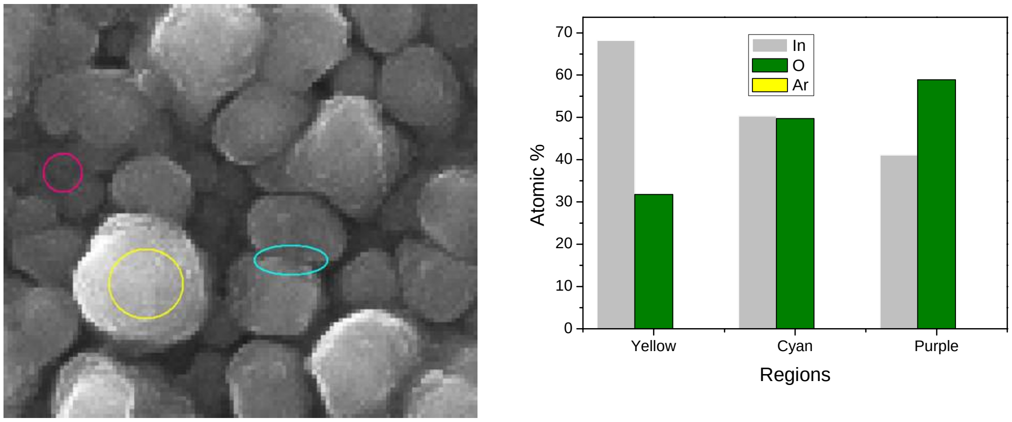

Figure 4.10: EDS analysis of sputtered indium film at low temperature.

Argon trap on films were not found, but a lot of oxide was captured by EDS analysis. Since SiO2 is under the layer of indium thin film, it is hard to say that the oxidation of indium during deposition affected the granular microstructure to cause impurity. Based on the condition of the above EDS results, it was intuited that oxidation occurred on the single layer of indium or around each grain. This hypothesis is illustrated in Figure 4.11. To investigate the shift and impurity effects on the microstructure of indium film, deeper study such as TEM should be performed.

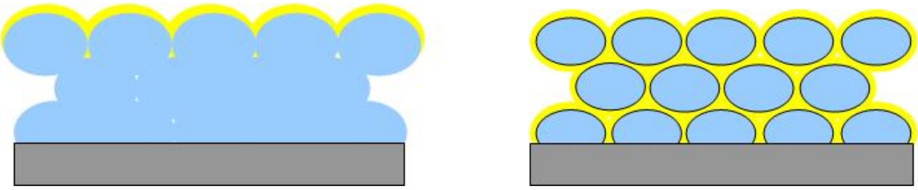

(a) (b)

Figure 4.11: Illustration of oxidation of indium on a) surface and b) grain boundary

4.2.5 Modified Nano-grain size through diffusion control

Due to cryogenic cooling substrate, the roughness of film was dramatically improved by the power of influence on low temperature, and roughness was improved four times less than that of film deposited at room temperature (see Figure 4.12).

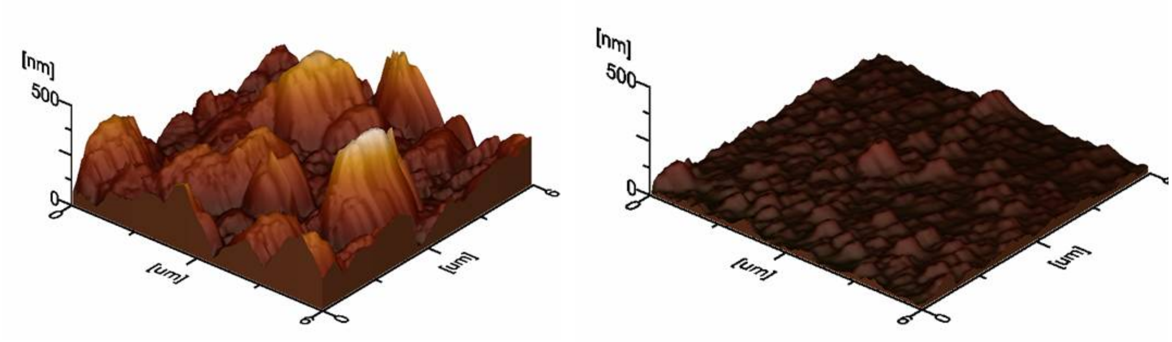

(a) (b)

Figure 4.12: Compared SPM 3-D images. Films are deposited at a)298K (90.1 nm), and b) 163 K (15.1 nm).

At low temperature, the effects of the number of impinging atoms and energy of atoms were investigated by changing power and pressure respectively. Sputtering power was increased from 100 W to 150 W, and surface morphology was shown in Figure 4.13.

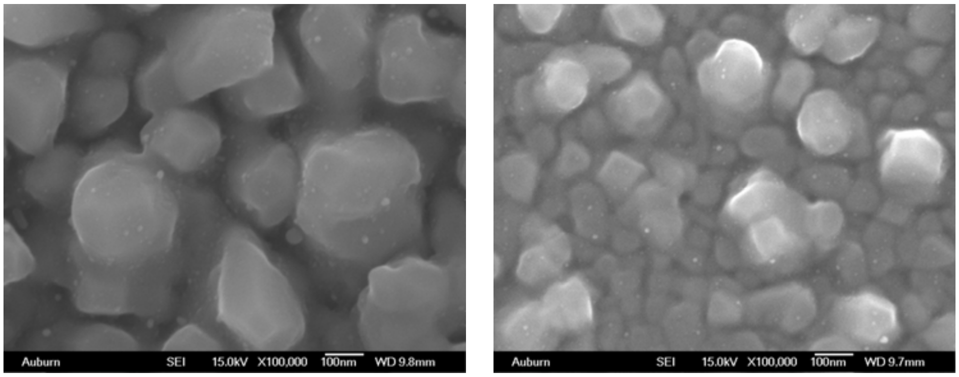

(a) (b)

Figure 4.13: Compared SEM images of sputtered indium films at low temperature with different DC power as a) 100W and b) 150W, and under 75 mTorr pressure

Nucleation dominant growth of film made grain size smaller with increasing number of impinging adatoms or deposition rate. Also, increasing pressure reduced the energy of adatoms, and restricted diffusion created smaller grain size with dominated nucleation process (see in Figure 4.14)

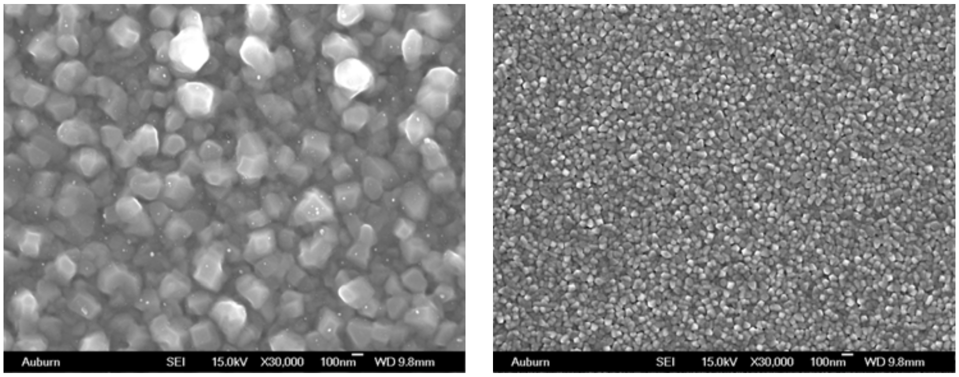

(a) (b)

Figure 4.14: Compared SEM images of sputtered indium films at low temperature with different process pressure as a) 5 mTorr and b) 14 mTorr, and under 100W DC power

These microstructure evolutions agreed well with previous results that were deposited at room temperature with changing deposition rate and energy of adatoms.

4.3 XRD analysis for film stress

As shown in SEM images, indium film formed polycrystalline, with a body-centered tetragonal (bct) crystallographic structure based on Joint Committee on Powder Diffraction Standards (JCPDS) card, as shown in Figure 4.15. Indium has peaks in the order of (101)/(110)/(112)/(002), and their intensity ratio is 1/0.36/0.24/0.21 in bulk material. Body-centered tetragonal materials thermodynamically prefer to (101) plane due to its lower plane energy.

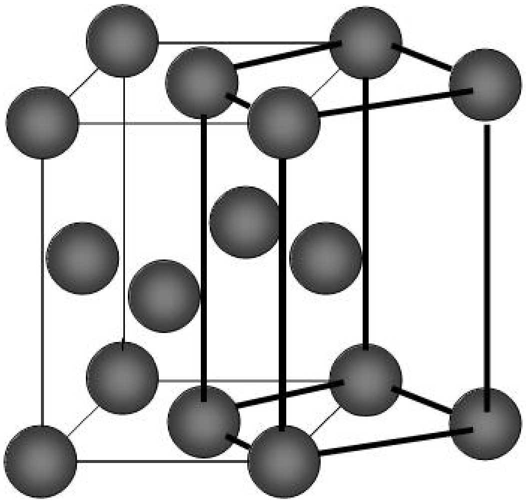

Figure 4.15: Body-centered tetragonal

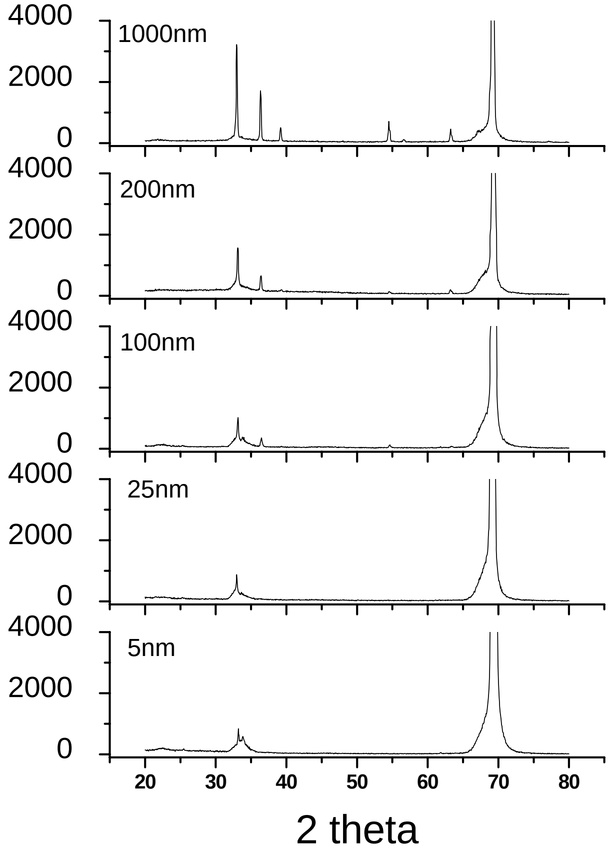

Figure 4.16: XRD results depends on the thickness of indium films

XRD characterizations were performed for indium films by increasing its thickness to 5, 25, 100, 200, and 1000 nm in Figure 4.16. Indium atoms were dominantly stacked on (101) plane with longer average resident time with lower potential energy on that plane than that of others.

The ratio of other planes such as (110), and (002) to (101) plane showed divergence from that of bulk indium material in JCPDS with higher and lower intensity respectively in Figure 4.17. This deviation is evidence of existing film stress that induces unfavorable orientation from thermodynamic equilibrium crystallographic orientation.

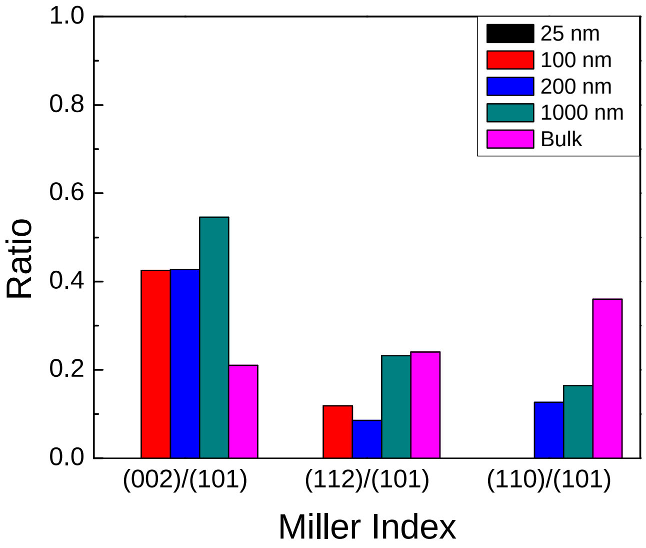

Figure 4.17: Comparison of ratio of intensity between low order planes and first peak plane.

Stress-induced rough surface also appeared in indium films deposited on amorphous and textured substrate such as SiC, Ti, and Cr in Figure 4.18. These results shows that rough surface morphology of low melting temperature material is not dependent on substrate material, but the internal stress of itself.

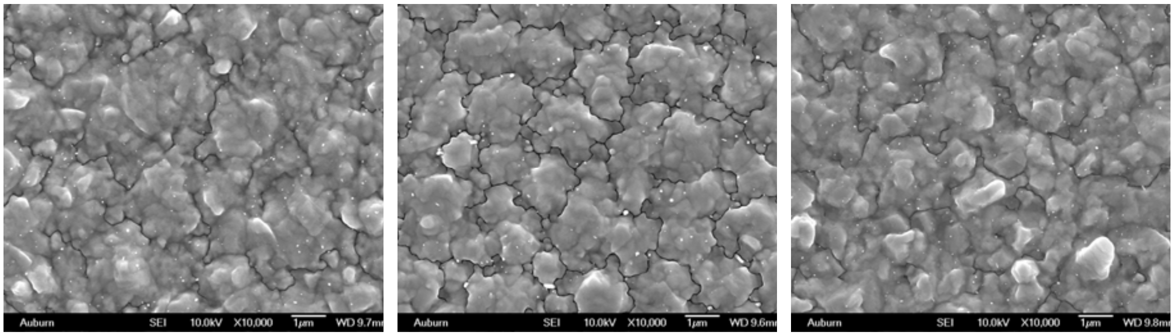

(a)In/SiC (b)In/Ti (c)In/Cr

Figure 4.18: Indium films on various interlayer (30nm)

Each grain is under stress by which low melting temperature materials can easily change its shape. This deformation of grains can be shown by changes of lattice parameter, and they can be simply calculated by the shift in XRD peaks in Equation 2.19.

Table 4.3: Lattice parameters on z-axis of (002) plane as thickness of films

	Bulk	100 nm	200 nm	1000 nm
a_z on (002)	2.4730	2.4739	2.4772	2.4706
Deviation	0	+0.0009	+0.0042	-0.0024

Vertical expansion of the unit cell means compressive strain in a lateral direction. Capillary force is one of the compressive stresses on film itself, and island growth is its stress relaxation. Percolation of grains limits relaxation of compressive stress, and then faucet surface appears. SEM analysis in Figure 4.1 shows good agreement.

As indium film deposited at room temperature was compared with that at low temperature, (002) peak intensity show less ratio value to the very first peak (101) on later film (seen in Figure 4.16).

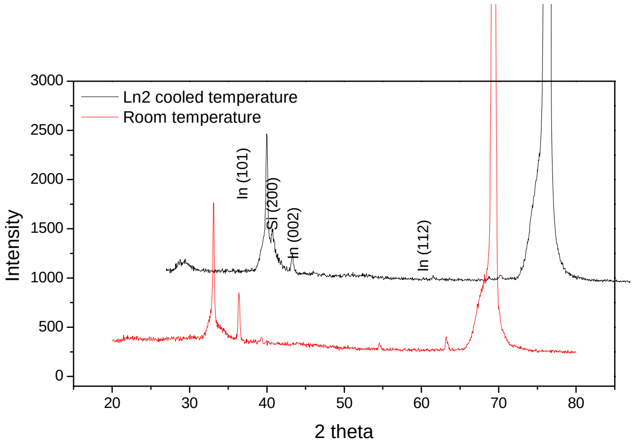

Figure 4.19: XRD data compared between films deposited at room temperature and low temperature

Table 4.4: Peak intensity ratio of indium system

	(101)	(002)	(002)/(101)
Bulk indium	100	21	0.21
Film at 163 K	1533	308	0.2009
Film at 298 K	1768	852	0.4819

.

Table 4.3 shows the intensity ratio between (101) and (002): the origin value of (002)/(101) ratio, 0.21, can be compared with that of each film.

Film deposited at 163 K has a more similar intensity ratio to that of bulk, and (101) texture was preferred to orient within lower plane energy in thermodynamic. In constrast, film deposited at 298 K has stronger intensity on (002) than that of bulk indium. This unstable orientation seems to be generated by stress during film formation. Faucets on SEM images might demonstrate relaxation of this stress; however, no faucets were found on the film deposited at low temperature.

If we assume that Young’s modulus and poison ratio of nano-scale grains are the same as that of bulk, stress of each film was measured by XRD with Equation 2.19.

When Young's modulus of indium is 10.6/GPa, and Poison ratio is 0.4498, 54 MPa of compressive stress was loaded on the film deposited at room temperature. Films deposited at low temperature showed no stress with perfect coincidence between peak angles of real peak and JCPDS peak. Also, internal stress of indium films deposited at room temperature can be calculated with the assumption in Figure 4.20.

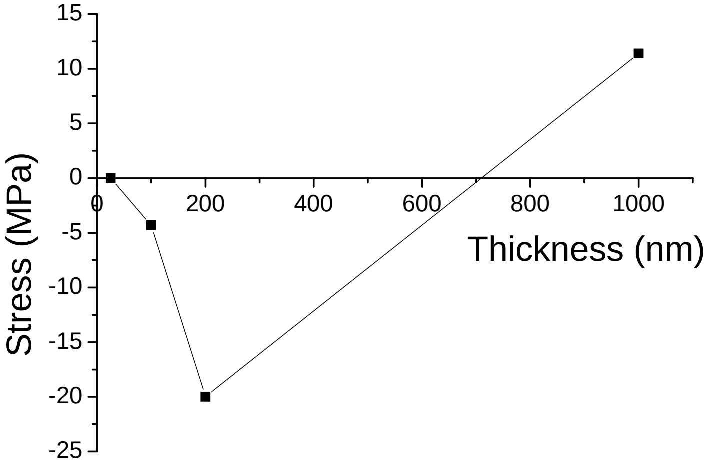

Figure 4.20: Stress analysis of indium films deposited at room temperature with the assumption that Young's modulus and Poison ratio is the same as that of bulk.

4.4 Optical characterization of indium film

Microstructure is the factor with the most impact on optical properties, and optical properties of film can be a way of characterizing the microstructure in the contrary. Previously mentioned indium films with modulated microstructure were characterized by measuring reflectance. Films were directly deposited on slide glass or photodiode, and photocurrent was compared before and after blocking the diode. When reflectance of film that deposited on slide glass was measured by the change of the photocurrent with filtering, slide glass turned upside down to exclude deflection caused from rough surface of film, and to prevent leakage of light from side of glass. Photocurrent changes as thickness was explored with room light source in Figure 4.17.

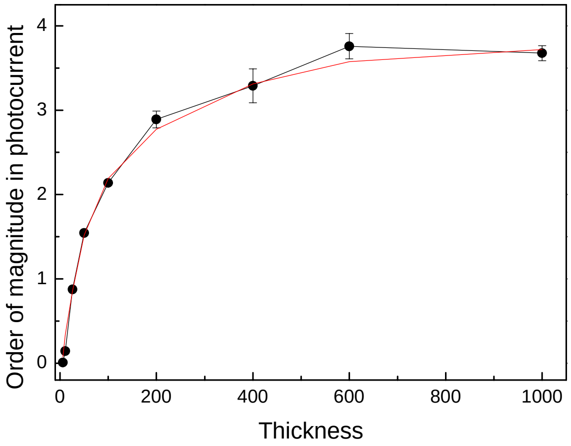

Figure 4.21: Reflectance changes as thickness of indium film changes under visible light. Film was deposited at room temperature with 100W (DC) and 5.2 mTorr

Indium films with different thickness ranging from 5 to 1000 nm were deposited at room temperature, and the photonic current of each film was measured at the out of chamber right after deposition. Reflectance was expressed in order of magnitude: the current on photodiode was reduced by reflecting incident visible light through indium films compared with current without film.

Under the result of reflectance versus film thickness, reflectance showed rapid increase up to 400 nm thickness of film. Reflectance seemed to be saturated at this thickness up to measured thickness of films. Based up on SEM analysis in the previous section, the steep gradient was caused from the open channel region before percolation and the relative thinner region at grain boundary after percolation due to large faucet-shaped grain. Although thickening of the film seemed to lead to saturation of reflectance with homologous microstructure, rough surface morphology conserved or worsened during thickening in Figure 4.2-a.

Reflectance of indium films that had various surface morphology induced by process parameter changes were measured to investigate the relationship with roughness. Roughness was improved by the nucleation dominant process (see Figure 4.3) with high deposition rate, and indium films were deposited at the same process parameters except pressure. Since high chamber pressure crates a high probability of collision between target atoms and ionized gas molecules, the energy of diffusion of adatoms on the surface is kinetically restricted. As roughness and reflectance of indium films deposited at 5, 10, 14 mTorr were measured in Figure 4.18, reflectance increased with shrinkage of rough surface morphology induced by groovy grain boundary.

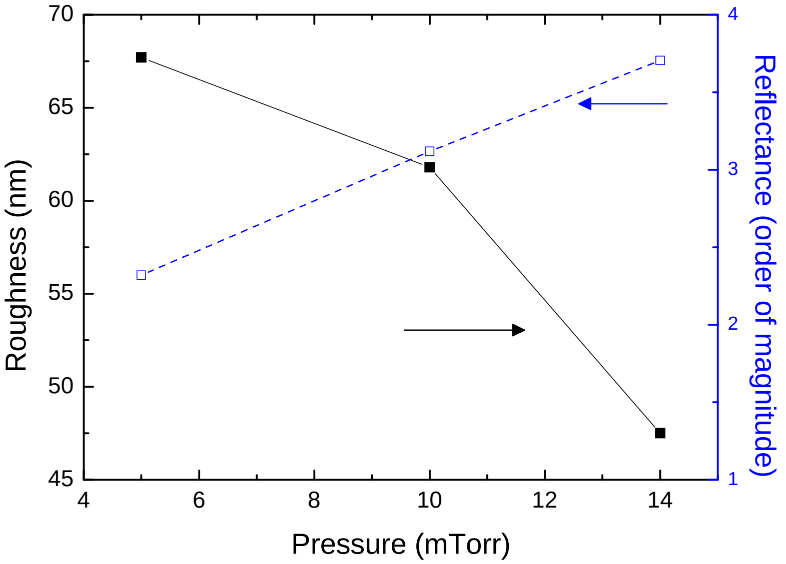

Figure 4.22: Roughness and reflectance of indium film depends on process pressure. Indium was deposited on holder position, and thickness of 165 nm.

As shown in Figure 4.9, deposited indium film under low temperature had continuous and uniform film at the thickness of 200 nm. Its roughness was improved to 15.1 nm by cooled substrate temperature and decreased diffusion energy of adatoms through high processing pressure. Film was directly deposited on the photodiode with 200 nm, and photocurrent was measured. Reflectance was also improved to 4.55 in order of magnitude, and its high value was much higher than that of 1000 nm thick film deposited at room temperature. It seemed that leakage of visible light though thinner region at groovy grain boundary was diminished, and reflection at grain boundary and expected micro-voids caused this high value.

The rough surface of deposited film at a too high temperature can be submitted as an issue in optical thin film application that mostly requires uniform morphology. In contrast, very fine grain also induces degradation of optical properties of thin film due to increments of grain boundary and micro-voids.

4.5 Electrical characterization of indium films

Sheet resistance of indium thin film was measured to characterize microstructure, and to compare effects of grain boundary with that of poor uniformity in metallic interconnect application. Four point probe measurement was used against indium films deposited on 10x10 mm SiO_2/Si pieces, and deposited at room temperature and liquid nitrogen cooled temperature in Figure 4.19.

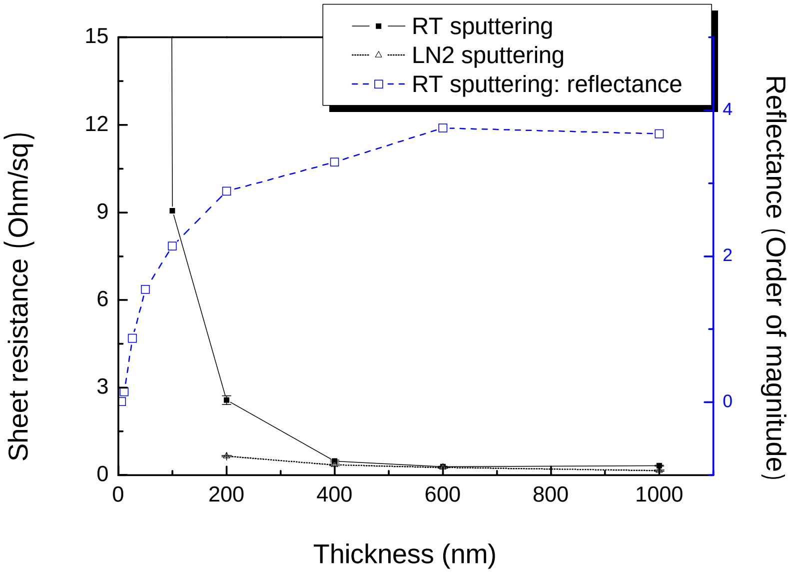

Figure 4.23: Sheet resistance of indium films deposited at room temperature and liquid nitrogen-cooled temperature

Indium films deposited at room temperature reached percolation thickness around 100 nm in Figure 1. From Figure 4.20, reflectance and sheet resistance began to saturate at a thickness of 400 nm. After comparison with the percolation thickness of other metallic films as at a few tenths of thickness, the percolation and saturation thickness of indium thin film was relatively thicker at a few hundredths. It seemed that very groovy grain boundary primarily affected this phenomenon. The microstructure of thin film mostly influences resistance in two aspects: the thickness variation in uniformity of thin film and the ratio of grain boundary. Based on SEM analysis, parabolic plot and saturation of sheet resistance was supposed to be caused from faucet-shape grain.

Indium film deposited at liquid nitrogen-cooled temperature showed relatively a uniform surface and large area of grain boundary with fine-grained microstructure. Since sheet resistance of film deposited at low homologous temperature had smaller change with thickness than that of film deposited at high homologous temperature, the rough surface was supposed to seriously influence optical and electrical properties of thin film in comparison to grain boundary effect.

4.6 Revised SZM

The microstructure of thin film can be mostly interpreted by the diffusion energy of adatoms, and most SZMs deal with homologous temperature, pressure, and bias in thickness (>1μm) deposited by the PVD method. While surface temperature supports diffusion of atoms on the surface of sample and film itself during deposition, other variables are closely related to the energy of impinging adatoms.

As thinner films are required by the present technology, SZM for thin (<1μm) film was built up with revising the previous Grovenor's SZM. Also, deposition rate was added on this model, since it is well known that a high number of impinging atoms without consideration of their energy induces microstructure evolution with nucleation dominant film formation. Indium was sampled due to its low melting temperature, and Al and Pb were applied on this model to generalize it. Revised SZM was built up and proposed with consideration of homologous temperature, gas pressure, and deposition rate in sputter deposited thin film with thickness ranging up to 1 μm in Figure 4.20.

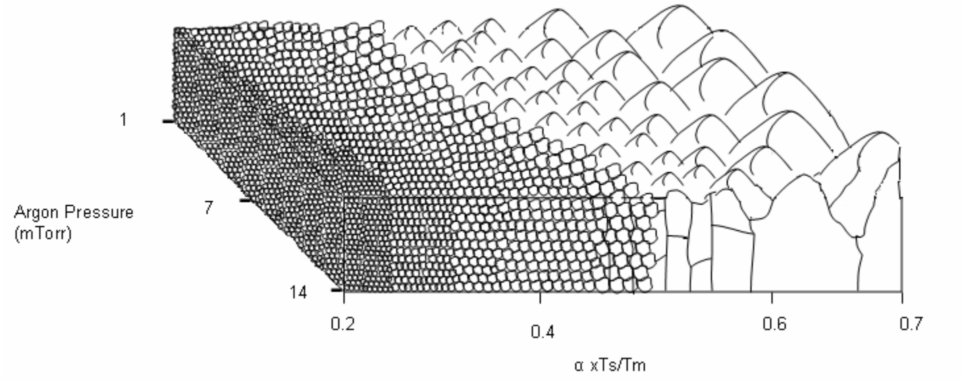

Figure 4.24: Revised Structure Zone Model

Indium thin film deposited at less than 0.4 homologous temperature had fine microstructure with a large number of grains throughout.

CHAPTER 5

SUMMARY AND CONCLUSIONS

Indium thin films were grown on amorphous substrate by a magnetron sputtering system to obtain continuous and uniform microstructure in very thin film applications. Film microstructure was effectively modulated by changing process parameters such as power, pressure, and substrate temperature in a sputtering system. Smooth surface with small grain size was obtained by restricting diffusion of atoms and by increasing nucleation rate. Among process parameters, temperature was the most influential parameter. Sputter deposition of low melting temperature material at cryogenic temperature enabled homologous temperature at a lower range, and resulted in development of granular structure with fine grains less than 80 nm. Indium thin films deposited at room temperature corresponding to higher homologous temperature produced very rough surface morphology due to compressive strain induced during deposition. It is believed that the sources of compressive strain result from thermal stress and intrinsic stress during film formation enhanced by high diffusivity of atoms in low melting temperature materials. Low resistivity and high reflection characteristics were obtained on films deposited at cryogenic temperature, and their values show clear improvement when compared with values on relatively thick films deposited at high homologous temperature.

The experimental results have reasonable agreement with the proposed SZM by Grovenor in which granular structure existed at low homologous temperature. The upper boundary of granular structure shifted from 0.2 to 0.5 homologous temperature in sputter deposited indium. Since impurity effects were not found in EDS analysis, it is considered that different adatom energy and kinetic effects depending on different system geometry and conditions may lead to different zone range.

Future work will be to understand what factors determine columnar and granular structure on film deposited at low homologous temperature, and its boundary shift.

BIBLIOGRAPHY

1. Ohring, R.R.a.M., Void formation and growth during electromigrationi in thin films. J. Appl. Phys., 1971. 42: p. 5671-5679.

2. E. G. Vil'kin, L.v.L., and A. V. Pashuk, A solar blind filter for the ultraviolet spectral range. Inst. Exp. Tech., 2001. 44: p. 121-122.

3. Forbes R. Powell, P.W.V., Joakim F. Lindblom, and Stephen F. Powell, Thin film filter performance for extreme ultraviolet and x-ray applications. Optical Eng., 1990. 29: p. 614-624.

4. w. R. Hunter, D.W.A., and R. Tousey, Thin films and their uses for the extreme ultraviolet. Applied Optics, 1965. 4: p. 891-898.

5. S. Aggrawal, A.P.M., S. R. Perusse, R. Ramesh, V. Ballarotto, E. D. Williams, B. R. Chalamala, Y. Wei, R. G. Reuss, Spontaneous ordering of oxide nanostructures. Science, 2000. 287: p. 2235-2237.

6. Grovernor, C.R.M., The development of grain structure during growth of metallic films. Acta Metall., 1984. 32: p. 773.

7. Ohring, M., Materials Science of Thin Films. Second ed. Deposition & Structure. 2002: Academic Press.

8. Rodbell, J.M.E.H.a.K.P., Microstructure control in semiconducture metallization. J. Vac. Sci. Technol. B, 1997. 15: p. 763.

9. S. P. Riege, J.A.P., and A. W. Hunt, Influence of microstructure on electromigration dynamics in submicron Al interconnects: Real-time imaging. Appl. Phys. Lett., 1996. 69(16): p. 2467.

10. Plummer J.D., D.M.D., Griffin P.B., Silicon VLSI Technology Fundamentals. Practice and Modeling. 2000: Prentice Hall.

11. Forbes R. Powell, P.W.V., Joakim F. Lindblom, Stephen F. Powell, Thin film filter performance for extreme ultraviolet and x-ray applications. Optical Engineering, 1990. 29(6): p. 614.

12. Hummel, R.E., electronic Properties of Materials. 3rd ed. 2000, NY: springer-Verlag. 199-224.

13. M. Harris, H.A.M., S. Ogura, E. Pelletier, and B. Vidal, The relationship between optical inhomogeneity and film structure. Thin Solid Films, 1979. 57: p. 173.

14. Guenther, K.H., Physical and chemical aspects in the application of thin films on optical elements. Applied Optics, 1984. 23(20): p. 3612.

15. W. T. Perrins, D.R.M., and R. C. McPhedran, Transport properties of regular array of cylinders. Proc. R. Soc. London Ser. A, 1979. 369: p. 207.

16. Guenther, P.G.W.a.K.H., Accurate and precise reflectance measurement of highly reflecting mirrors. Topical Meeting on Optical Interference, 1984: p. Paper WA-C1.

17. Powell, F., Care and feeding of soft x-ray and extreme ultraviolet filters. Laser-induced Damage in Optical Materials, 1992. 1848: p. 503.

18. Guenther, K.H., Microstructure of vapor-deposited optical coatings. Applied Optics, 1984. 23(21): p. 806.

19. Grill, A., Cold plasma in materials fabrication from jundamentals to applications. 1993, Piscataway, NJ: IEEE PRESS.

20. Thompson, C.V., Structure Evolution During Processing of Polycrystalline Films. Annu. Rev. Mater. Sci., 2000. 30: p. 159-190.

21. Pashley, D.W., The growth and structure of gold and silver deposits formed by evaporation inside an electron microscope. Philos. Mag., 1964. 10: p. 127-158.

22. D. Walton, T.N.T., and R. W. Rollins, Nucleation of silver on sodium chloride. J. Chem. Phys, 1963. 38(11): p. 2698-2704.

23. Demchishin, B.A.M.a.A.V., Study of the structure and properties of thick vacuum condensates of Nickel, Titanium, Aluminium Oxide and Zirconium Dioxide. Phys. Met. Metallogr., 1969. 28: p. 83.

24. Thornton, J.A., High rate thick film growth. Ann. Rev. Mater. Sci., 1977. 7: p. 239.

25. Thornton, J.A., Influence of apparatus geometry and deposition conditions on the structure and topography of thick sputtered coatings. J. Vac. Sci, 1974. 11: p. 666.

26. R. Messier, A.P.G., and R. A. Roy, Revised structure zone model for thin film physical structure. J. Vac. Sci. Technol. A, 1984. 2: p. 500.

27. Grovernor, C.R.M., The development of grain structure during growth of metallic films. Acta Metall., 1984. 32: p. 773.

28. R. Messier, S.V.K., L.R. Gilbert, and P. Swab, Black A-Si solar Selective Absorer Surfaces. J. Appl. Phys., 1980. 51(3): p. 1611-1614.

29. P. Swab, S.V.K., and R. Messier, Characterization of Black Ge Selective Absorbers. J. Vac. Sci. Technol. A, 1980. 17(1): p. 362-365.

30. J. A. Thornton, D.W.H., Stress related effects in thin films. Thin Solid Films, 1989. 171: p. 5-31.

31. Hoffman, R.W., Physics of Thin Films. 3rd ed. Advances in Research and Development, ed. G.H.a.R.E. Thun. Vol. 3. 1966, New York: Academic Press.

32. R. Koch, D.W.a.K.H.R., Intrinsic stress of epitaxial thin films. Physica Scripta, 1993. T49: p. 539-543.

33. Abermann, R.K.a.R., Microstructureal changes in vapour-deposited silver, copper and gold films investigated by internal stress measurements. Thin Solid Films, 1986. 140: p. 217-226.

34. Chaudhari, P., Grain growth and stress relief in thin films. J. vac.Sci. Technol., 1971. 9: p. 520-522.

35. C. W. Mays, J.S.V.a.D.k.-W., On surface stress and surfce tension: II. Determination of the surface stress of gold. Surface science, 1968. 12(2): p. 134-140.

36. B. Moraweck, G.C.a.A.J.R., contraction and relaxation of interatomic distances in small platinum particles from extended X-ray absorption fine structure (EXAFS) spectroscopy. Surface Science, 1979. 81(2): p. L631-L634.

37. Cammarata, R.C., Surface and interface stress effects in thin films. Progress in Surface Science, 1994. 46(1): p. 1-38.

38. Koch, R., The intrinsic stress of polycrystalline and epitaxial thin metal films. Condens. Matter, 1994. 6: p. 9519-9550.

39. R. Abermann, R.K.a.R.K., Electron microscope structure and internal stress in thin silver and gold films deposited onto MgF2 and SiO substrates. Thin Solid Films, 1979. 58(2): p. 365-370.

40. Koch, R.A.a.R., In situ study of thin film growth by internal stress measurement under ultrahigh vacuum conditions: Silver and copper under the influence of oxygen. Thin Solid Films, 1986. 142(1): p. 65-76.

41. R. Koch, D.W., A. Fuhrmann, and K. H. Rieder, Growth-mode-specific intrinsic stress of thin silver films. Phys. Rev. B, 1991. 44(7): p. 3369-3372.

42. Windischmann, H., Intrinsic stress in sputter-deposited thin films. Crit. Rev. Solid State Mater. Sci, 1992. 17(6): p. 547-596.

43. Thornton, D.W.H.a.J.A., Internal stresses in Cr, Mo, Ta, and Pt films deposited by sputtering from a planar magnetron source. J. Vac. Sci. Technol., 1981. 20(3): p. 355-358.

44. Hoffman, D.W., Perspective on stresses in magnetron-sputtered thin films. J. Vac. Sci. Technol. A, 1994. 12(4): p. 953-961.

45. R. W. Vook, Int. Metals Rev., 1982 27:p.209